Effect of microfabrication processes on surface roughness parameters and micro/nanoscale friction behavior of silicon surfaces

by

Sharath Chandrasekaran

A thesis submitted to the graduate faculty

in partial fulfillment of the requirements for the degree of

MASTER OF SCIENCE

Major: Mechanical Engineering

Program of Study Committee:
Sriram Sundararajan (Major Professor)
Pranav Shrotriya
Gary Tuttle

Iowa State University

Ames, Iowa

2004

Graduate College

Iowa State University

This is to certify that the master's thesis of

Sharath Chandrasekaran

has met the requirements of Iowa State University

Signatures have been redacted for privacy

TABLE OF CONTENTS

Chapter 1. General introduction

1.1 Surface roughness and nanotribological characterization of MEMS surfaces

Micromechanical system (MEMS) refers to devices with at least some of their dimensions in the micrometer range. The advances of photolithographic process technology since 1960 have led to the development of MEMS. These processes are being complemented with nonlithographic micromachining processes for fabrication of milliscale components or devices. Using these fabrication processes, researchers have fabricated a wide variety of miniaturized devices, such as acceleration, pressure and chemical sensors, linear and rotary actuators, electric motors gear trains and gas turbines, nozzles, pumps fluid valves, switches gripers, tweezers, and optoelectronic devices with dimensions in the range of a couple to a few thousand microns. The success of silicon in MEMS devices can be attributed to the available fabrication technology of integrated circuits. Mechanical stability is crucial for mechanical applications of these MEMS devices [1]. Any MEMS device must be free of drift to avoid recalibration at regular intervals. Part of the drift in mechanical sensors may be associated with movement of crystal dislocations in the loaded mechanical part. In ductile materials such as metals, dislocations move readily. By contrast, in brittle materials such as semiconductors, dislocations hardly move. Mechanical engineers often avoid brittle materials and opt for ductile material even though these plastically deform, meaning that they are subjected to mechanical hysterisis. Single crystal silicon can be made virtually without defects and, under an applied load no dislocation line can move. This means that at room temperature, Si can be deformed elastically. This last property, coupled with an extremely

high yield strength (comparable to steel), makes Si a material preferred to any metal in most MEMS applications. As a consequence Si has been widely used as a structural element in MEMS. Pressure and acceleration sensors based on simple piezoresistive elements embedded in a silicon movable mechanical member, have turned into major commercial applications. Silicon based acceleration sensors are used in anti-skid braking systems and four wheel drives. Acceleration sensor technology is slightly less than a billion-dollar-a-year industry dominated by Lucas NovaSensor and Analog Devices. Silicon based pressure sensors are used for monitoring pressure of cylinders in automotive engines and of automatic tires. The area in which MEMS has one of its biggest commercial breakthroughs lately are in micro machined mirrors for optical switching in both fiber optics communication [2] and data storage applications [3]. Optical switches are to optical communications what transistors are to electronic signaling. What makes Si single crystal attractive in this case is the optical quality of the Si surface. The quality of the mirror surface is primordial to obtain very low insertion loss even after multiple reflections. Figure 1 shows examples of MEMS devices. Fig 1(a) is a microchain fabricated at the Department of Energy's Sandia National Laboratories and it closely resembles a bicycle chain except that each link could rest comfortably atop a human hair. Fig. 1(b) shows microscopic canals on chips, through which liquids or gases can flow from one chip feature to another. Such canals are useful for emerging families of miniscule gadgets called "microfluidic" devices that make use of the chemical properties of liquids or gases and the electrical properties of semiconductors on a single chip or among nearby chips. Fig 1(c) shows a high performance MEMS-Based 8x8-Port Optical Switch.

Fig 1(a) Sandia silicon microchain demonstrates engaging simulated device drive gears (Sandia national labs).

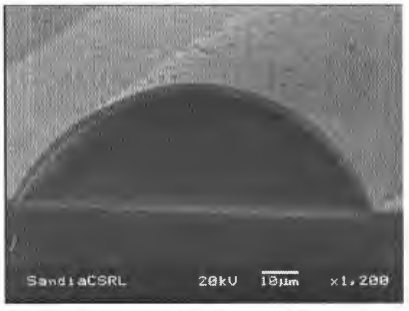

Radius of curvature: 52 µm

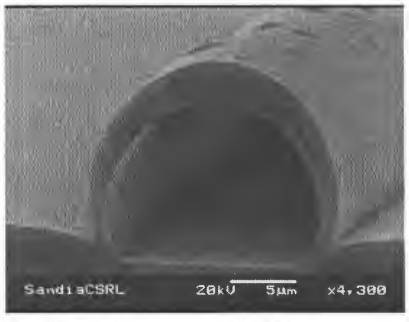

Radius of curvature: 8 µm

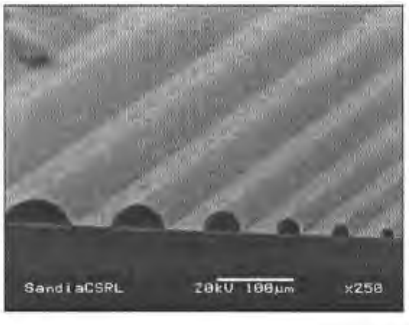

Fig 1 (b) Microscopic views of raised, hemispherical canals ranging from 8 to 100 microns in diameter. A human hair is about 100 microns across (Sandia national labs).

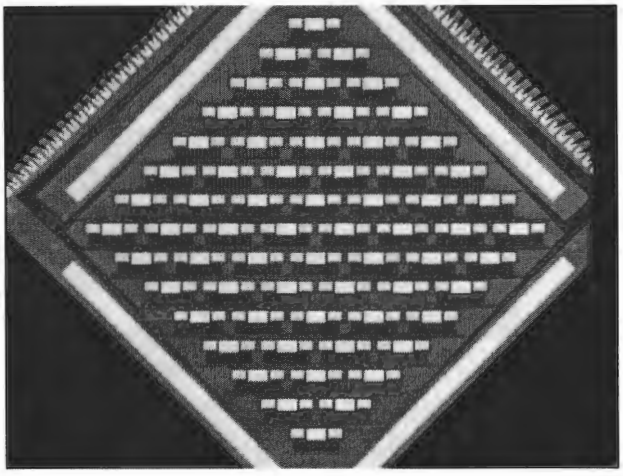

Fig 1(c) High Performance MEMS-Based 8x8-Port Optical Switch (Horsley et al., 2003)

Etching has long been used for fabricating microstructures such as diaphragms and cantilevers on a silicon wafer. The demands for complicated 3-D microstructures on a silicon chip are growing in such fields as ink-jet printing devices and microfluidic systems. Improved anisotropic etching technologies using computer simulation have allowed precise compensation of mask-patterns, multi-step etching processes, and optimization of etchant conditions [4]. However, these technologies have been focusing mainly on the product shape and not on the quality of the surface. The roughening of the silicon surface caused by etching needs to be studied to evaluate the quality of the etched device surface. Surface roughness of mating surfaces also affects the tribological behavior of the interface. Several studies have shown that tribology (friction, wear and lubrication) is a critical factor undermining the reliability of MEMS devices. Hence there is a need to quantify surface roughness parameters of microfabricated silicon surfaces and understand their effect on tribological behavior. Very few studies have been focused on the roughness analysis and tribological comparison of the etched surfaces.

1.2 Micro/Nanotribology –significance and application

The word tribology is derived from the Greek word "tribo" meaning rubbing and "logy" meaning knowledge. The original applications by the Greeks were in trying to understand the motion of large stones across the earth's surface. Today tribology has grown to include the methodical study of friction, lubrication, and wear.

Tribology plays a critical role in diverse technological areas. In the advanced technological industries of MEMS, semiconductor and data storage, tribological studies help optimize polishing processes and lubrication of data storage substrates. In traditional industries such as

automotive and aerospace, tribological studies help increase the lifespan of mechanical components.

Many industrial processes including MEMS fabrication require a detailed understanding of tribology and at the nanometer scale it is referred to as nanotribology. This field is concerned with experimental and theoretical investigations of processes ranging from atomic and molecular scale to microscale, occurring during adhesion, friction, wear, and thin film lubrications at sliding surfaces [5]. These studies are needed to develop fundamental understanding of interfacial phenomenon in micro and nanostructures used in micromechanical systems and other industrial applications. The components used in micro and nanostructures are very light (on the order of a few micrograms) and operate under very light loads. As a result, friction and wear of lightly loaded micro/nano components are highly dependent on surface interactions. These surfaces are generally lubricated with molecularly thin films. Micro and nano tribological techniques are ideal to study friction and wear processes of micro-nano structures. These studies are also valuable in the fundamental understanding of interfacial phenomenon in macro structures to provide a bridge between science and engineering. Friction and wear on the nano scale have been found to be generally smaller compared to that at microscale. Therefore, micro-nano tribological studies may identify regimes for ultra low friction and zero wear.

There are a number of traditional tools for characterizing friction, lubrication and wear. The most common characterization tool is the tribometer having several configurations such as pin-on-disk, ball on flat, and flat on flat, etc. On the microscopic scale of surface measurements, a contact type stylus profiler (SP) using electronic amplification is the most popular [6]. In SP, the stylus is loaded on the surface to be measured and then moved across

the surface at a constant velocity to obtain surface height variation. Generating motion at the nanometer scale is extremely challenging. New characterization techniques are required to understand tribology at the nanometer scale.

1.3 Scanning probe microscope

The best suited instrument for micro/nanotribology is the family of surface probe microscopes or SPMs, which are derived from scanning tunneling microscopes (STM). The scanning tunneling microscope developed by Dr. Gerd Binning and his colleagues in 1981 was the first instrument capable of directly obtaining three dimensional images of solid surfaces with atomic resolution [7]. But the STM was capable of studying surfaces that were electrically conductive. By combining the STM design with the concept of the stylus profiler, Binning et al developed the atomic force microscope (AFM) in 1985, to measure ultra small forces (1μN) present between the AFM tip and the sample surface [8,9]. The atomic force microscope is now being routinely used to study nanoscale tribology. The natural extension of the AFM for tribology applications is derived from the motion of a nanometer-sized stylus in the AFM over a surface. Although traditional tribology testing is not done with an AFM, many new types of applications are possible.

Examples of the application of AFM in tribology include:

- *Surface characterization of morphology, texture, and roughness.*

The AFM gives extremely high contrast on surfaces that are flat at the nanometer scale. Optical and electron microscopes are not able to resolve surface texture that is easily measured with the AFM. Applications include the visualization of surface topography in both 2-D and 3-D perspective, line roughness measurements and area roughness measurements.

All the traditional area and surface roughness parameters can be calculated after the AFM image is acquired [6,10,11].

- *Measurement of friction forces at the nanometer scale.*

Friction between two surfaces depends on the chemical and mechanical interaction between the surfaces. Changes in chemical composition giving rise to friction are measurable with the AFM. The technique for measuring these forces is called lateral force, or frictional force microscopy. As the probe moves over a surface in the AFM, changes in the chemical composition of the surface can give rise to torsions of the cantilever on which the probe is mounted. The torsion of the cantilever is then proportional to the friction between the probe and the surface [12,13]. The friction response of the tip on a sample is the difference between the lateral deflection values of forward and reverse scans of a given scan line (i.e. from the friction loop of a scan line). This method is commonly used to eliminate contributions from non-friction sources [5]. The friction value thus noted is a measure of the friction force.

- *Measuring lubricity.*

The probe is mounted on the end of the cantilever in an AFM making it possible to measure interaction forces between the probe and the surface by monitoring the deflection of the cantilever [14]. A graph, called the force-distance curve shows the forces on the probe as the distance between the probe and the surface is reduced. The nature of the force distance curves depends on the force constant of the cantilever, lubrication density, probe geometry and the lubrication thickness. By measuring the changes in force distance curves in an AFM it is possible to directly ascertain the thickness of the lubrication films.

- *Generation of scratch and wear tracks and direct three-dimensional visualization of wear tracks or scars on a surface.*

The effect of wear at the nanometer scale becomes critical to the optimization and stability of machines as the tolerance in precision machines become smaller and smaller. The AFM can be used to investigate scratch and wear resistance of the surface [3,15,16]. The AFM also allows direct 3-dimenional visualization of the wear tracks [17]. The image may be displayed in a 2-D projection and a 3-D projection. Direct measure of wear track depth can be easily measured with a line profile derived from the AFM image.

- *Evaluation of mechanical properties such as hardness and elasticity, and plastic deformation at the nanometer scale.*

Mechanical properties such as hardness, elastic modulus, stiffness and compressibility as well as mechanical behavior such as plastic deformation, and fracture can be studied with the AFM [18,19]. It is possible to study nanohardness by directly pressing an AFM probe into a sample surface; however, it is advantageous to use an instrument that is optimized for nanoindentation . The primary advantage of the nano-indentor over an AFM for nano-hardness measurements is that it is easier to get calibrated measurements with the nanoindentor. It is useful to use an AFM to measure three-dimensional topography of the indentations made with the nano-indentor. AFM images allow direct visualization of material deformation or fracture behavior.

A major advantage of the AFM for tribological studies is that the AFM can be routinely used on all types of materials. Materials commonly studied include: ceramics, metals, polymers, semiconductors, magnetic, optical, and biomaterials. AFM investigations are usually made in ambient air environment. It is possible to make AFM studies in vacuum and liquid environment.

1.4 Research objectives

Several studies have shown that the choice of etchant, etchant concentration, temperature and silicon crystallographic direction affects the roughness of the resulting surfaces Most of these studies have used optical microscopy or scanning electron microscopy to qualitatively evaluate the roughness of the etched surfaces. However a complete descriptive evaluation of surface roughness parameters was not sought. Very few studies have been focused on the roughness analysis of the etched surfaces. The research objective of this study is to evaluate the effect of selected etchants and additives on the surface roughness parameters of the resulting etched silicon surfaces using atomic force microscopy and profilometry. Micro/nanoscale friction behavior of the surfaces was also evaluated. Correlations in the friction behavior and surface roughness parameters are discussed.

1.5 Thesis organization

The thesis is presented in the form of two papers. Both the papers follow the same format: an abstract, followed by an introduction, experimental details, results and discussion, conclusions and references. Following the second paper is a chapter giving general conclusions.

In Chapter 2, the effects of different etchants on the surface roughness of a Si (100) surface were investigated using atomic force microscopy. We studied the effect of tetra methyl ammonium hydroxide (TMAH), KOH (6M, 8M and 10M) and deep reactive ion etching (DRIE) on the surface roughness parameters of the resulting silicon surfaces. To provide a full description of the surface geometry both the amplitude (RMS, peak to valley distance, skewness, and kurtosis) and spatial parameters (autocorrelation length) were evaluated.

Using these measured values surfaces for low friction behavior is identified using a dry contact model developed by Kotwal and Bhushan [20].

In Chapter 3 we present our investigations on the effect of selected etchants and additives on the surface roughness parameters of the resulting etched silicon surfaces using atomic force microscopy and profilometry. Surface roughness evolution spectroscopy (SRES) analysis was carried out to determine the prominent frequencies that arise due to the etching processes. A dry contact model was used to predict real contact area of these surfaces. Single asperity and multiple asperity friction experiments of the surfaces were also carried out to evaluate differences in tribological behavior due to difference in roughness. Correlations between observed tribological behavior and surface roughness parameters are discussed.

Finally, all the conclusions of the studies conducted are presented in Chapter 4.

1.6 References

1. M. J. Madou, Fundamentals of Microfabrication, CRC Press, New York, 2nd edn. 2002, p.212.

2. T. Li, M. Xiang and Y. Wang, "Electrostatic driven self-aligned optical switch", Proceedings of SPIE-The International Society for Optical Engineering, 4602 (2001) 9.

3. B. Bhushan, B. K. Gupta and M. H. Azarian, "Nanoindentation, Microscratch, Friction and Wear Studies of Coatings for Contact Recording Applications", Wear, 181 (1995) 743.

4. K. Sato, M. Shikida, T. Yamashiro, K. Asaumi, Y. Iriye and M. Yamamoto, "Anisotropic etching rates of single-crystal silicon for TMAH water solution as a function of crystallographic orientation", Sensors and Actuators, A: Physical, A73 (1999) 131.

5. B. Bhushan, Handbook of Micro/Nano Tribology, CRC Press, 2nd edn 1999, 859 pp.

6. C. Y. Poon and B. Bhushan, "Comparison of surface roughness measurements by stylus profiler, AFM and non-contact optical profiler", Wear, 190 (1995) 76.

7. G. Binning, H. Rohrer, C. Gerber and E. Weibel, "Surface studies of Scanning Tunneling Microscope", Phys. Rev. Lett., 49 (1982) 57.

8. G. Binning, C. F. Quate and C. Gerber, "Atomic Force Microscopy", Phys. Rev. Lett., 56 (1986).

9. G. Binning, C. Gerber, E. Stoll, T. R. Albrecht and C. F. Quate, "Atomic resolution with Atomic Force Microscope", Europhys. Lett., 3 (1987) 1281.

10. S. Sundararajan and B. Bhushan, "Static friction and surface roughness studies of surface micromachined electrostatic micromotors using an atomic force/friction force microscope", J. Vac. Sci. Technol., A: Vacuum, Surfaces, and Films, 19 (2001) 1777.

11. R. Buzio, C. Boragno and U. Valbusa, "Contact mechanics and friction of fractal surfaces probed by atomic force microscopy", Wear, 254 (2003) 917.

12. S. Sundararajan and B. Bhushan, "Micro/nanotribological studies of polysilicon and SiC films for MEMS applications", Wear, 217 (1998) 251.

13. B. Shi, X. Lu, J. Luo, D. Chen and H. Liang, "Frictional properties of molecular thin films", Surface and Interface Analysis, 32 (2001) 283.

14. M. Salmeron, "Nanoscale wetting and de-wetting of lubricants with scanning polarization force microscopy", NATO Science Series, II: Mathematics, Physics and Chemistry, 10 (2001) 651.

15. M. Bai, K. Kato, N. Umehara, Y. Miyake, J. Xu and H. Tokisue, "Scratch-wear resistance of nanoscale super thin carbon nitride overcoat evaluated by AFM with a diamond tip", Surface and Coatings Technology, 126 (2000) 181.

16. S. Sundararajan and B. Bhushan, "Development of a continuous microscratch technique in an atomic force microscope and its application to study scratch resistance of ultrathin hard amorphous coatings", J. Mater. Res., 16 (2001)

17. A. Khurshudov and K. Kato, "Wear mechanism in reciprocal scratching of polycarbonate, studied by atomic force microscopy", Wear, 205 (1997) 1.

18. S. Sundararajan, B. Bhushan, T. Namazu and Y. Isono, "Mechanical property measurements of nanoscale structures using an atomic force microscope", Ultramicroscopy, 91 (2002) 111.

19. C.-C. Lee and W. Hsu, "Method on surface roughness modification to alleviate striction of microstructures", Journal of Vacuum Science & Technology, B:

Microelectronics and Nanometer Structures--Processing, Measurement, and Phenomena, 21 (2003) 1505.

20. C. A. Kotwal and B. Bhushan, "Contact analysis of non-Gaussian surfaces for minimum static and kinetic friction and wear", Tribology Transactions, 39 (1996) 890.

Chapter 2. Effect of microfabrication processes on surface roughness parameters of silicon surfaces

\ To appear in Surface Coatings and Technology

Sharath Chandrasekaran, Sriram Sundararajan

2.1 Abstract:

Surface roughness parameters affect the real area of contact and hence the friction in micro/nanoscale systems. Few studies have addressed the interplay between surface roughness of processed surfaces using prevalent microfabrication processes and their anticipated tribological behavior. In this paper, the effects of different etchants on the surface roughness of a Si (100) surface were investigated using atomic force microscopy. The etchants studied were TMAH (25% aqueous at 90 °C) and KOH solution (6M, 8M and 10 M at 80 °C). The surfaces generated by these wet-etching techniques were compared with the surface generated by deep reactive ion etching (DRIE). Quantitative surface roughness parameters (RMS, peak-to-valley distance, skewness, kurtosis and autocorrelation length) of the various surfaces were obtained from atomic force microscope images at different scan sizes. Results showed that DRIE produced the smoothest etched surface while TMAH produced the roughest surface. 8 M KOH produced smoother surfaces than 6 M and 10 M solutions. A dry contact model based on using the Pearson system of curves to generate the probability density function from the measured roughness parameters was used to estimate real area of contact and number of contacts for the various surfaces. From the contact model we find that DRIE and 6 M KOH surfaces show the least number of contacts and are therefore the preferred etching methods to realize surfaces with minimum adhesion/friction.

2.2 Introduction:

Etching processes play a key role in silicon-based fabrication of microstructures. A wide variety of anisotropic etchants have been used for etching Si surfaces such as potassium hydroxide (KOH), sodium hydroxide (NaOH), lithium hydroxide (LiOH), cesium hydroxide (CsOH) and ammonium hydroxide (NH_4OH) [1]. KOH is a popular etchant because it produces a uniform and bright surface [1]. Since SiO_2 is often used as a mask to etch Si, TMAH aqueous solutions are very favorable due to their very good etch selectivity between Si and SiO_2. One of the crucial issues during the etching process is its effect on the surface roughness of the resulting etched silicon film surface. The roughening of Si (100) surfaces caused by etching can affect their nanotribological (friction and wear) behavior [2,3] as well as mechanical properties of microscale structures[4-6]. Few studies have been carried out to measure the roughness of the etched surfaces [7-10]. Experiments have shown that the roughness of the etched surface depends upon the temperature and concentration of the etchants [9,10]. Etching of Si surfaces with KOH has been studied before to determine the effect of crystallographic orientation and also the effect of etching parameters like solution concentration and temperature [11]. However the authors have not performed detailed evaluation of surface roughness of the resulting surfaces. In this study we use atomic force microscopy to study the effect of TMAH, KOH and deep reactive ion etching (DRIE) on the surface roughness parameters of the resulting silicon surfaces. To provide a full description of the surface geometry both the amplitude (RMS, peak to valley distance, skewness, and kurtosis) and spatial parameters (autocorrelation length) were evaluated. Using these measured values surfaces for low friction behavior are identified using a dry contact model developed by Kotwal and Bhushan [12].

2.3 Experimental details:

In all the experiments, n-type silicon (100) wafers were used. The wafers were cut into 1 cm × 1cm samples and cleaned using the RCA standard clean process [13] before and after etching to remove the surface contaminants. Hydrogen fluoride (HF) solution was not used during this cleaning process as the removal of the oxide film exposed the Si surface to metallic impurities [14]. The etchants studied were TMAH and KOH. A 25% aqueous solution of TMAH was used at 90 °C. KOH solutions with concentrations ranging from 6 to 10 M were used at a temperature of 80 °C. A SiO_2 layer was used as a mask to determine the etch rates of the various etchants. Wafers were thermally oxidized to an oxide thickness of 300 nm and patterns were developed using photolithography to expose a square region of Si. After the etching process with various etchants the SiO_2 mask was removed by dipping the samples in HF solution. Etch depth analysis was carried out using a profilometer. All the samples were etched to a depth of about 10 μm. After etching with the anisotropic etchants the quality of the surface was poor due to the deposition of the reaction products on the wafer surface [9]. The reaction products were removed using an SPM clean (H_2SO_4:H_2O_2 = 4:1, 90°C) followed by dipping the samples in 37% HCl. The surfaces obtained after the cleaning process were of excellent quality with no contamination. Samples etched using deep reactive ion etching (DRIE), a dry etch process that allows the creation of vertical structures with high aspect ratios and extensive design freedom were also studied. DRIE was done using an ALCATEL 601E system which uses a patented high density inductively coupled plasma (ICP) source and a fluorine based non-corrosive etch chemistry (BOSCH process).

Surface roughness of the etched Si (100) samples was determined using an atomic force microscope (AFM, Dimension^{TM} 3100, Nanoscope IV). Surface imaging was carried out in

tapping mode under ambient conditions (25 °C, 40%RH) using a silicon tip (tip radius of about 10 nm) at scan sizes of 1 μm ×1 μm, 5 μm ×5 μm and 20 μm×20 μm with a resolution of 256×256 data points per scan.

2.4 Results and discussions:

The etch rate for the TMAH solution was 0.62 μ/min. The etch rates for 6 M KOH, 8 M KOH and 10 M KOH were determined to be 1.4 μ/min, 1.2496 μ/min and 1.0587 μ/min. The etch rates obtained are comparable to previously measured etch rates [1,9]. Fig. 1 shows typical AFM topography maps obtained on unetched Si (100) at scan sizes of 1 μm × 1 μm, 5 μm × 5 μm and 20 μm × 20 μm. The polished Si wafer has very low roughness and hence there are no discernable features on the surface. Also shown in Fig. 1 are the Si (100) surfaces etched with TMAH and by DRIE. The TMAH surface is highly textured and shows the presence of pits at larger scan sizes. The surfaces obtained after DRIE are extremely smooth and do not show much texture. Fig. 2 shows topography maps of Si surfaces etched using 6 M, 8 M and 10 M KOH solutions. KOH-etched surfaces exhibit pit-like structures at higher scan sizes.

Surfaces with a non-Gaussian distribution and exponential autocorrelation function can be characterized using the amplitude parameters root mean square (RMS) roughness, maximum peak to valley distance (PTV), skewness (Sk), kurtosis (K), and the spatial parameter: autocorrelation length [15].

For a surface height distribution (z) whose probability density function is given by p(z), the root mean square (RMS or R_q) is the square root of the arithmetic mean of the square of the vertical deviations from the reference line as shown below:

$$RMS^2 = \int_{-\infty}^{\infty} z^2 p(z)dz \qquad (1)$$

Maximum peak to valley distance (PTV) is the distance between the highest asperity and deepest valley of the surface. Skewness (Sk) represents the degree of symmetry of the height distribution about the mean and is equal to the normalized third moment of p(z) about the mean line:

$$Sk = \frac{1}{\sigma^3} \int_{-\infty}^{\infty} (z-m)^3 p(z)dz \qquad (2)$$

where m is the mean line of the surface heights and σ is the variance. Note that for a mean line of zero $\sigma = R_q$. Kurtosis (K) represents the peakedness of the height distribution and is a measure of the number of isolated peaks in the height distribution. Kurtosis is equal to the normalized fourth moment of p(z) about the mean line:

$$K = \frac{1}{\sigma^4} \int_{-\infty}^{\infty} (z-m)^4 p(z)dz \qquad (3)$$

A Gaussian surface has a skewness of zero and a kurtosis of three. Autocorrelation length (ACL) is a measure of randomness of the surface and is the length over which the autocorrelation function [15] drops to 1/e of its original value.

Fig. 3 shows the variation of RMS, PTV, skewness and kurtosis as a function of scan size for the etched surface and the unetched Si (100). All surfaces have slight non Gaussian characteristics. The values reported are averages of six measurements at different locations of the sample. Error bars are ± standard deviation. RMS roughness generally increases with scan size which is consistent with previously reported studies [16]. 6 M KOH and 10 M KOH etched surfaces showed highest RMS values at 1 μm scan size while 6 M KOH and TMAH etched surfaces showed highest roughness values at scan sizes of 5 μm and 20 μm.

The RMS roughness and PTV values for DRIE surfaces are fairly low and comparable to values obtained for unetched Si but show higher kurtosis and positive skewness. The roughness values for KOH etched surfaces have been shown to decrease with increasing concentration of the etchant solution [10]. Fig. 4 shows the variation of surface amplitude parameters as a function of the molar concentration of the solution for KOH-etched samples. We found that the RMS roughness is lower for 8 M KOH as compared to 6 M KOH but that 10 M KOH has higher roughness than 8M. 6 M KOH has positive skewness and high kurtosis compared to 8 M KOH and 10 M KOH surfaces which generally exhibit negative skewness. From Fig. 3, DRIE surfaces have positive skewness at all scan sizes and slightly high kurtosis at a scan size of 20 μm compared to the other surfaces. TMAH surface exhibits negative skewness and lower kurtosis compared to other surfaces at all scan sizes. Surfaces with positive skewness and higher kurtosis are known to exhibit lower real area of contact and hence lower friction [2,17]. Hence DRIE and 6 M KOH etched samples can be expected to exhibit low friction/adhesion properties.

Fig. 5 shows the spatial parameter, autocorrelation length as a function of scan size. For all samples the autocorrelation length gives the degree of randomness of the surface [15]. Surfaces with very high degree of randomness have high autocorrelation length. TMAH shows the highest autocorrelation length while DRIE shows the lowest autocorrelation length. All KOH etched samples showed comparable values.

We attempted to verify the contact behavior of these surfaces using a simple dry contact model developed by Kotwal and Bhushan [12]. Surface roughness causes contact to occur at discrete contact points which sums up to the real area of contact. When two rough surfaces are moved against each other, the adhesion between the asperities and other interactions at

these contact points affects the friction force between the surfaces [18,19]. For elastic contacts, which is usually the case for micro/nanoscale applications, the coefficient of adhesional friction μ_a is given by

$$\mu_a = \frac{A_r \tau_a}{W} \qquad (4)$$

where τ_a the interfacial shear strength, A_r is the real area of contact and W is the normal load [18]. In the elastic regime real area of contact and in turn friction force can be affected by changes in surface roughness[3]. Based on the Greenwood and Williamsons model [20] several analytical, numerical and fractal based contact models have been developed to estimate real area of contact [12,17,21] and friction [22] for rough surfaces. In order to estimate the real area of contact between a flat surface and the various etched surfaces we used a model developed by Kotwal and Bhushan for dry contact analysis [12]. This model uses the Pearson system of curves to obtain the probability density function. The Pearson system of frequency curves based on the method of moments provides a family of curves which can be used to generate an equation for a distribution for which the first four moments are known. Pearson defined a criterion *k* given by

$$k = \frac{\mathrm{Sk}^2 (\mathrm{K}+3)^2}{4(2\mathrm{K} - 3\mathrm{Sk}^2 - 6)(4\mathrm{K} - 3\mathrm{Sk}^2)} \qquad (5)$$

where *Sk* and *K* are the skewness and kurtosis of the surface as measured from topography scans. Depending on the value of *k* different equations can be obtained for the probability density function. For our entire sample set we obtained values of *k* close to zero and hence we used the following probability density function [12]:

$$p(z^*) = 0.3989 \exp(-0.5(z^*)^2) \qquad (6)$$

The probability density function is then used in the classical Greenwood and Williamson's model to obtain expressions for the real area of contact, number of contact spots and normal load in terms of the statistical parameters of the distribution [20]. The normal load (W), real area of contact (A_r) and the number of contacts (n) is given by [12]

$$W = \frac{4}{3}\eta A_a E' R_p \sigma_p^{1.5} F_{1.5}(h) \qquad (7)$$

$$A_r = \pi\eta A_a R_p \sigma_p F_1(h) \qquad (8)$$

$$n = \eta A_a F_0(h) \qquad (9)$$

The standardized separation h, is given by d/σ where d is the separation between the mean planes of the surfaces. E' is the equivalent young's modulus of elasticity and R_p is the equivalent radius of curvature. η, A_a and σ_p are the surface density of asperities, nominal contact area and the equivalent standard deviation of the peak asperities respectively and

$$F_n(h) = \int_h^{\infty} (s-h) p^*(s) ds \qquad (10)$$

where p* (s) is the height distribution scaled to make its standard deviation unity.

Using this contact model, graphs were plotted to show the variation of normalized real area of contact and normalized number of contacts as a function of normalized load for the different surfaces at 20 μm scan size as shown in Fig. 6. The normalized load is the term $\left[\frac{W}{\eta A_a E` R_p^{0.5} \sigma_p^{1.5}}\right]$; the normalized real area of contact is the term $\left[\frac{A_r}{\pi\eta A_a R_p \sigma_p}\right]$ and the normalized number of contacts is the term $\left[\frac{n}{\eta A_a}\right]$ which is obtained from equations (7), (8) and (9). From Fig. 6a it can be seen that the normalized real area of contact increases with

the normalized loads and that values obtained are comparable for all surfaces. However some differences are seen in the number of contacts formed for the various surfaces (Fig. 6b). 6 M KOH and DRIE etched samples show slightly lower number of contacts than 8 M and 10 M KOH etched samples and TMAH shows the highest number of contacts all the etched surfaces. Since normal load, real area of contact and number of contacts are normalized with local parameters, the slight differences between the various surfaces obtained from the model would be magnified in reality. In a humid environment, liquid menisci form at contact points between two surfaces. These menisci result in increased adhesive load between the contacting surfaces and hence a higher friction force [15]. Thus the etched surface with the least number of contact points would be preferable from a friction standpoint. Hence DRIE and 6 M KOH etched surfaces would be preferable for surfaces which require low friction/adhesion properties.

2.5 Conclusions:

This study compares micro/nanoscale surface roughness of silicon surfaces etched using various etching processes and predicts friction behavior based on a simple contact model. Results showed that DRIE produces the smoothest etched surface compared to the anisotropic etchants and also exhibits slightly lower number of contacts at a given load. Hence DRIE would be the preferred method for producing surfaces where surface roughness effects on mechanical properties need to be minimized (e.g. cantilever beams) as well as for surfaces requiring reduced friction/adhesion (e.g. for micromotors). 6 M KOH has high roughness and also exhibits high kurtosis and positive skewness and appears to be the best anisotropic etchant to produce surfaces with low friction. TMAH exhibits the highest

roughness, has the most random surface and also has the highest number of contact points compared to the other etchants. Hence, it should be least preferred to produce surfaces for minimal friction behavior. In future work we plan to study roughness effects due to etching of polysilicon and silica films and use a tribometer to conduct multi-asperity contact friction and wear studies on etched samples to verify predicted tribological behavior.

2.6 Acknowledgments:

The authors would like to thank Prof. Gary Tuttle at the Microelectronic Research Center at Iowa State University for his assistance in etching the samples and for engaging in several constructive discussions during the course of the work. Partial financial support for the study was provided by a University Research Grant from the Office of the Provost at Iowa State University.

2.7 References:

1. M. J. Madou, Fundamentals of Microfabrication, CRC Press, New York, 2nd edn. 2002, p.212.

2. R. Maboudian and R. T. Howe, J. Vac. Sci. Technol., B 15 (1997) 1.

3. S. Sundararajan and B. Bhushan, J. Vac. Sci. Technol., A: Vacuum, Surfaces, and Films, 19 (2001) 1777.

4. F. Ericson and J. A. Schweitz, J. Appl. Phys, 68 (1990) 5840.

5. T. Yi and C. J. Kim, Meas. Sci. Technol., 10 (1999) 706.

6. S. Sundararajan, B. Bhushan, T. Namazu and Y. Isono, Ultramicroscopy, 91 (2002) 111.

7. F. J. Williams, C. M. Aldao, Y. Gong and J. H. Weaver, Physical Review B: Condensed Matter, 55 (1997) 13829.

8. T. Baum and D. J. Schiffrin, J. Micromechanics and Microengineering, 7 (1997) 338.

9. I. Zubel, Sensors and Actuators, A: Physical, A70 (1998) 260.

10. M. Shikida, K. Sato, K. Tokoro and D. Uchikawa, Sensors and Actuators, A: Physical, A80 (2000) 179.

11. K. Sato, M. Shikida, T. Yamashiro, M. Tsunekawa and S. Ito, Sensors and Actuators, A: Physical, A73 (1999) 122.

12. C. A. Kotwal and B. Bhushan, Tribol. Trans., 39 (1996) 890.

13. G. K. Celler, D. L. Barr and J. M. Rosamilia, Electrochemical and Solid-State Letters, 3 (2000) 47.

14. R. Divan, N. Moldovan and H. Camon, Sensors and Actuators, A: Physical, A74 (1999) 18.

15. B. Bhushan, Principles and Applications of Tribology, John Wiley & Sons, Inc., NY, 1999, p. 99.

16. V. N. Koinkar and B. Bhushan, J. Appl. Phys, 81 (1997) 2472.

17. S. K. Chilamakuri and B. Bhushan, J. Eng. Trib, 212 (1998) 19.

18. F. P. Bowden and T. D, Clarendon press, Oxford (1950, 1964).

19. B. Bhushan, Handbook of Micro/Nano Tribology, CRC Press, 2nd edn 1999, 859 pp.

20. J. A. Greenwood and J. B. P. Williamson, Proc. R.Soc., A 295 (1966) 300.

21. W. Yan and K. Komvopoulos, J. Appl. Phys, 84 (1998) 3617.

22. R. Buzio, C. Boragno and U. Valbusa, Wear, 254 (2003) 917.

2.8 Figure captions:

Fig 1 AFM topography images of unetched Si (100), TMAH and DRIE etched surfaces at scan sizes of 1 μm, 5 μm and 20 μm respectively.

Fig 2 AFM topography images of Si (100) surface etched with 6 M KOH, 8 M KOH and 10 M KOH etchants at scan sizes of 1 μm, 5 μm and 20 μm respectively.

Fig 3 Variation of surface roughness amplitude parameters as a function of scan size for various etched samples. (a) RMS, (b) peak to valley distance (PTV), (c) skewness and (c) kurtosis.

Fig 4 Variation of surface roughness amplitude parameters as a function of molar concentrations of KOH etchant. (a) RMS, (b) peak to valley distance (PTV), (c) skewness and (c) kurtosis.

Fig 5 Autocorrelation length as a function of scan size for various etched surfaces.

Fig 6 Results of dry contact model for various etched surfaces. (a) normalized real area of contact and (b) normalized number of contacts as a function of normalized load.

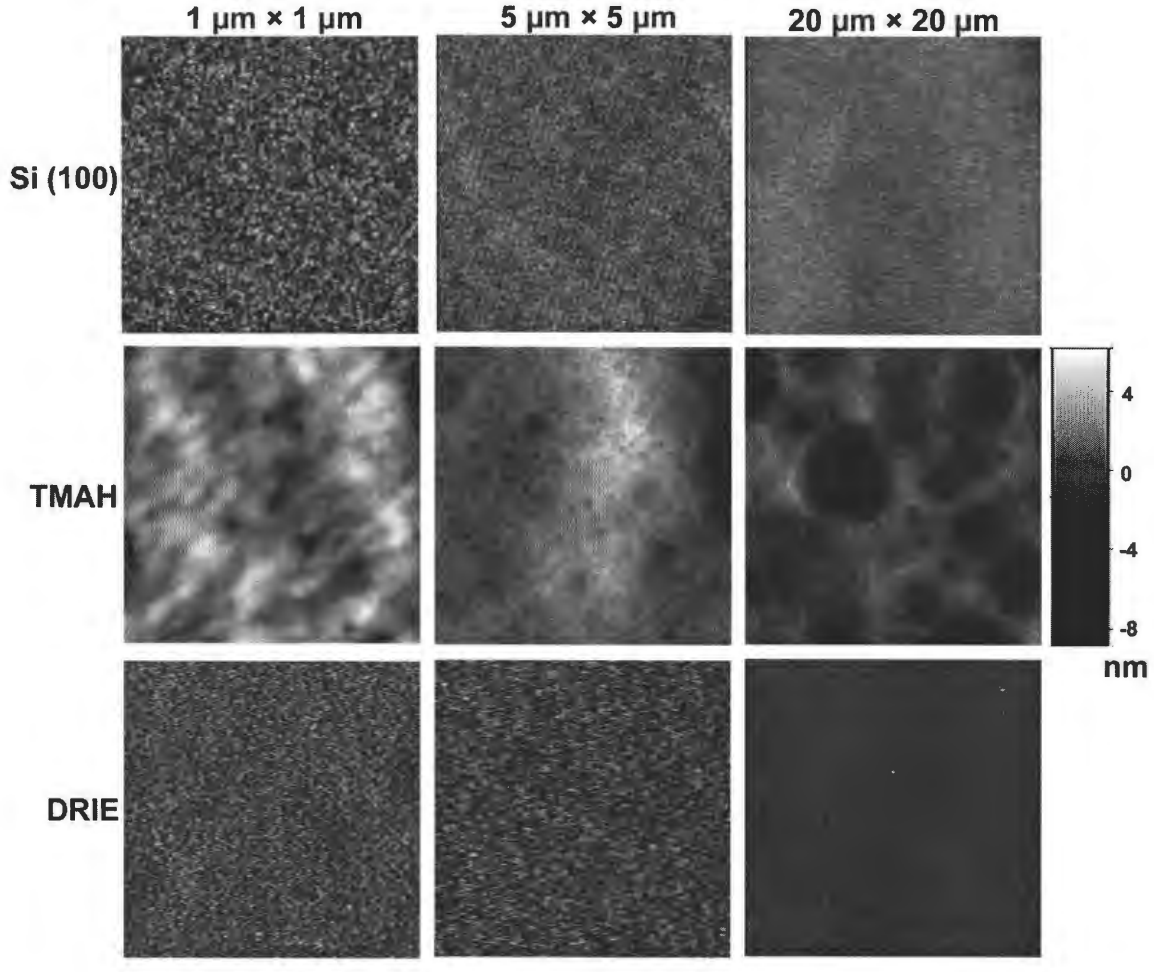

Fig 1

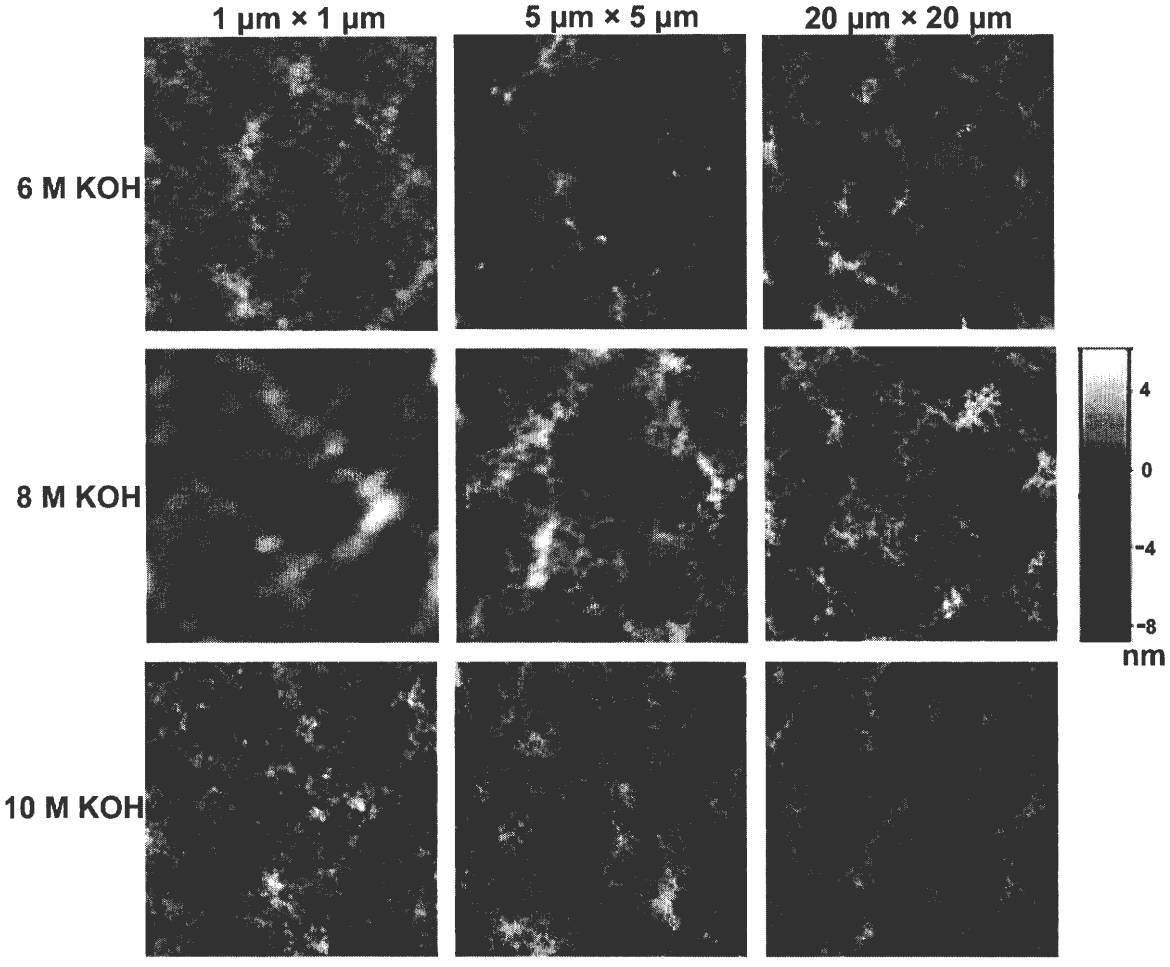

Fig 2

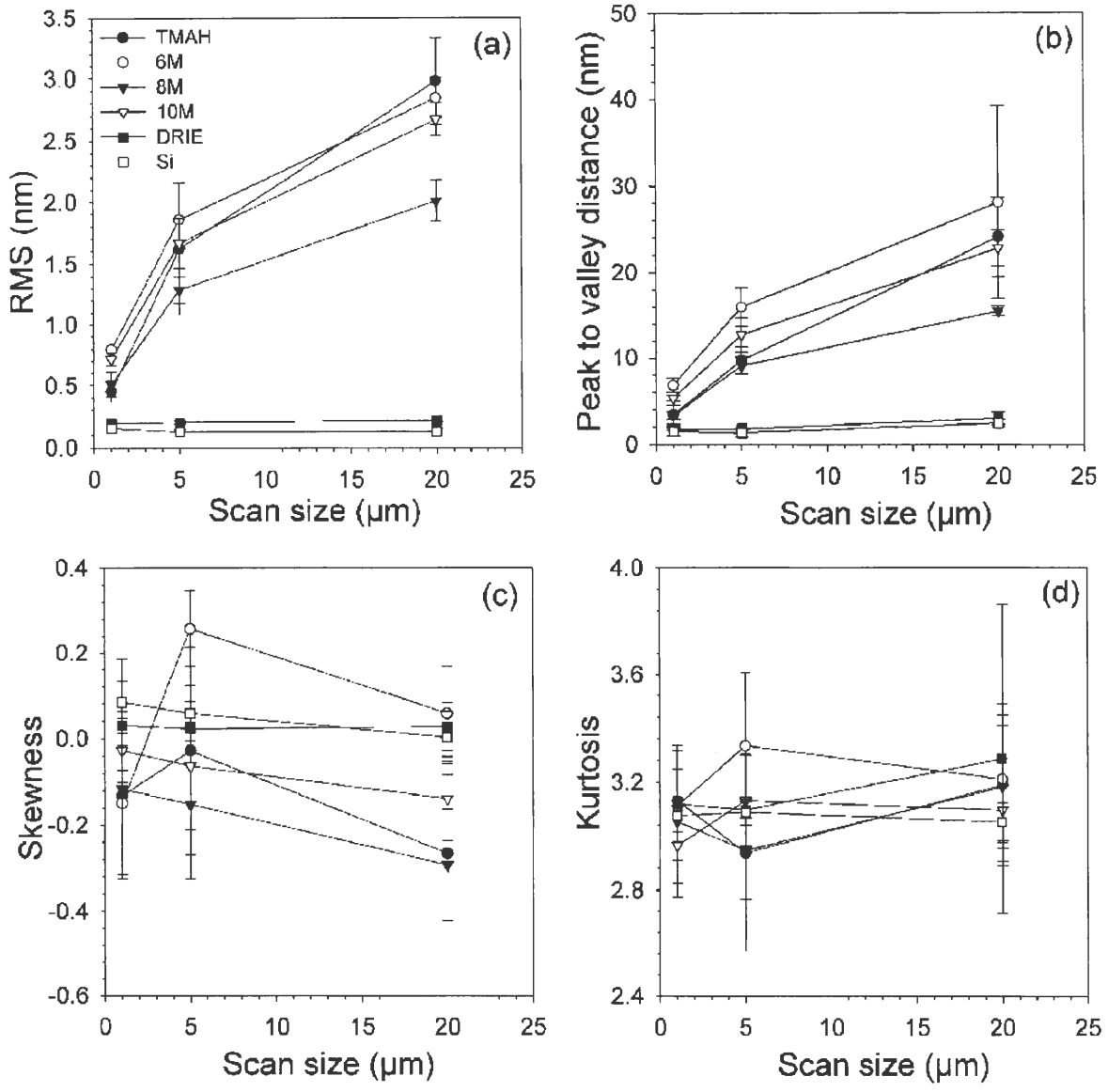
(a)
TMAH
6M
8M
10M
DRIE
Si
RMS (nm)
Scan size (μm)
(b)
Peak to valley distance (nm)
Scan size (μm)
(c)
Skewness
Scan size (μm)
(d)
Kurtosis
Scan size (μm)

Fig 3

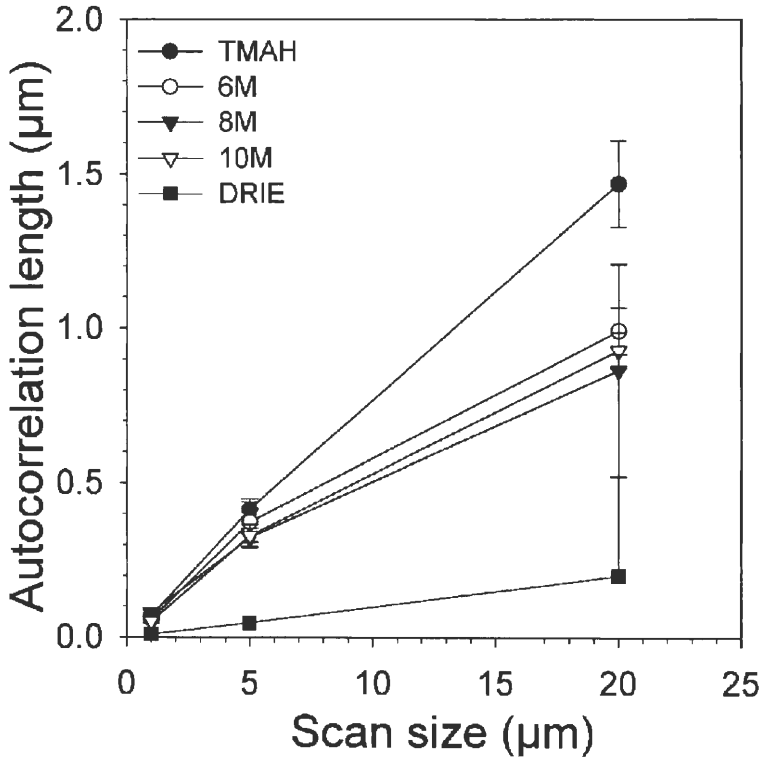
2.0
1.5
1.0
0.5
0.0
Autocorrelation length (μm)
TMAH
6M
8M
10M
DRIE
0
5
10
15
20
25
Scan size (μm)

Fig 4

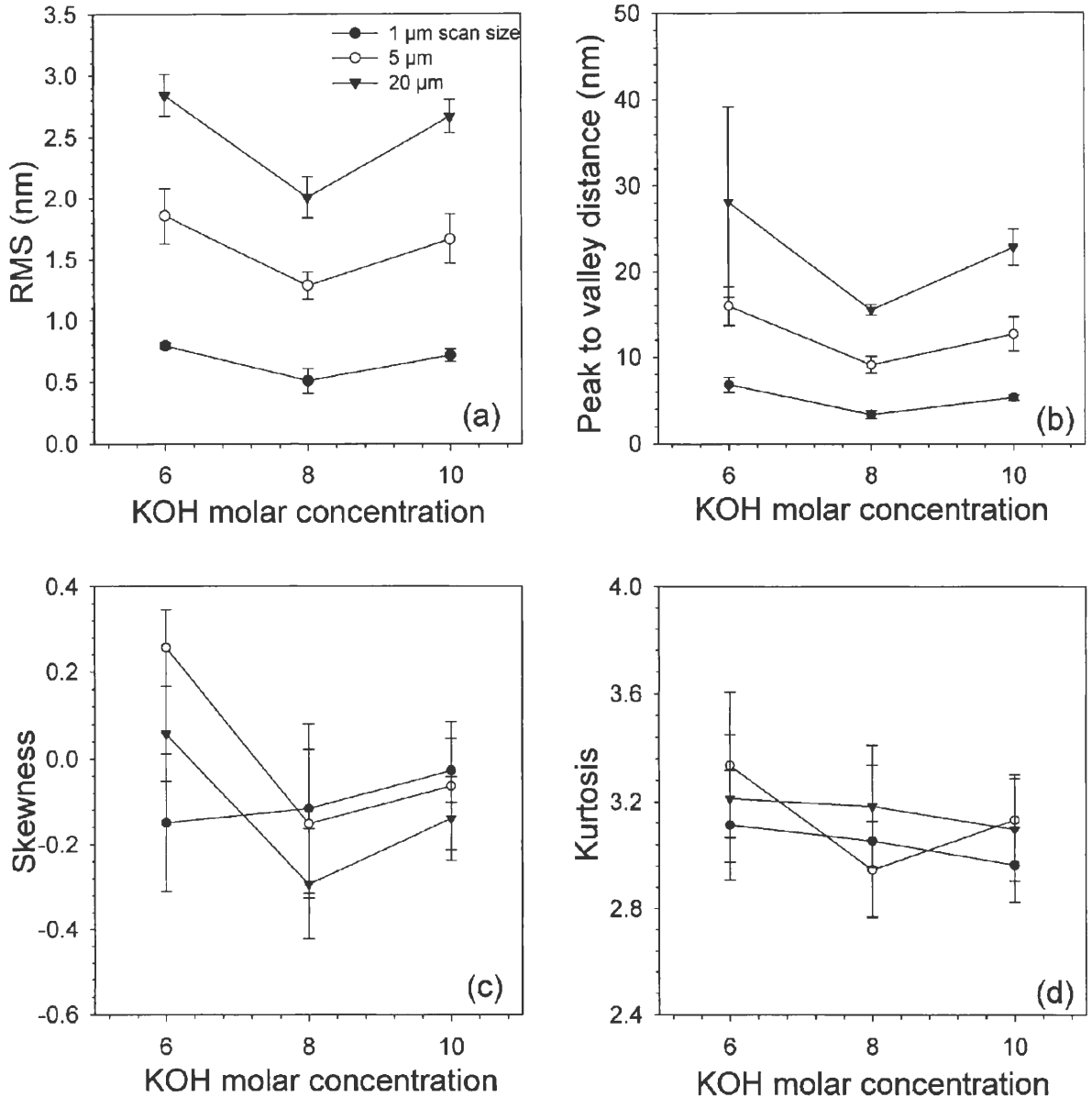
1 μm scan size
5 μm
20 μm
RMS (nm)
3.5
3.0
2.5
2.0
1.5
1.0
0.5
0.0
(a)
6
8
10
KOH molar concentration
Peak to valley distance (nm)
50
40
30
20
10
0
(b)
6
8
10
KOH molar concentration
Skewness
0.4
0.2
0.0
-0.2
-0.4
-0.6
(c)
6
8
10
KOH molar concentration
Kurtosis
4.0
3.6
3.2
2.8
2.4
(d)
6
8
10
KOH molar concentration

Fig 5

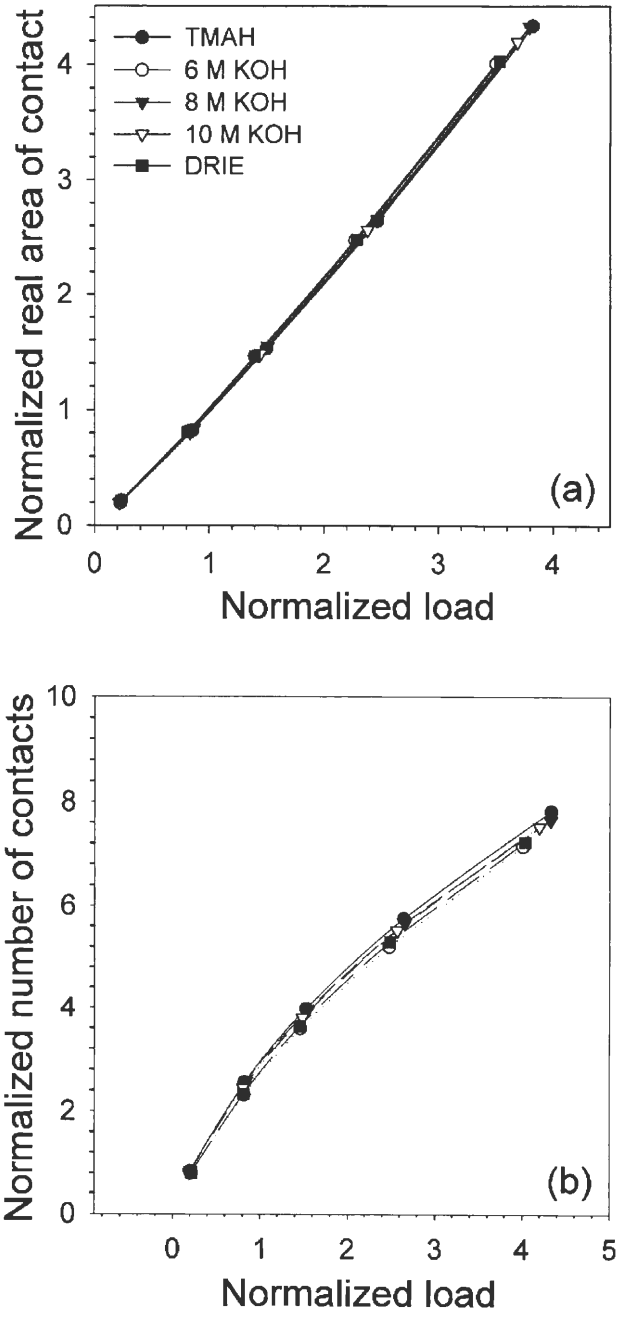
TMAH
6 M KOH
8 M KOH
10 M KOH
DRIE
Normalized real area of contact
Normalized load
(a)
Normalized number of contacts
Normalized load
(b)

Fig 6

Chapter 3. The effect of anisotropic wet etching on the surface roughness parameters and micro/nanoscale friction behavior of Si (100) surfaces

A paper submitted to Sensors and Actuators A

S. Chandrasekaran, J. Check, S. Sundararajan* and P. Shrotriya

3.1 Abstract:

Etching process can affect the surface roughness and hence the tribological properties of silicon surfaces. In this paper, we evaluate the surface roughness parameters and micro/nanoscale friction behavior of Si(100) surfaces etched using 8M KOH and tetramethyl ammonium hydroxide (TMAH) solution with and without isopropyl alcohol (IPA) additive. Amplitude and spatial parameters were evaluated using atomic force microscopy (AFM) and profilometry at scan sizes ranging from 1 μm to 500 μm. Results showed that TMAH and KOH produced comparable roughness up to 5 μm scan size and that at larger scan sizes, TMAH produced rougher surfaces than KOH. The use of IPA additive caused enhancement of sub-micron roughness features as well as a reduction in the long-range roughness of the surfaces resulting in smoother surfaces than the pure etchants. All etched surfaces exhibited pit like features with TMAH producing slightly larger pits than KOH. Surface roughness evolution spectroscopy (SRES) showed that using IPA resulted in an increase in the maximum pit size. Single asperity friction behavior correlated well with the adhesive forces for the various surfaces - KOH and TMAH showed comparable behavior and the use of IPA resulted in lower friction forces. However the use of IPA resulted in surfaces with higher real area of contact, which was responsible for higher friction forces in multiple asperity contacts on the microscale. This study demonstrates that the choice of etchants and additives affect the surface roughness and microscale friction behavior of the resulting surfaces.

3.2 Introduction:

Surface topography and roughness are important parameters affecting the mechanical [1-4] and tribological [5,6] behavior of structures and devices in microelectromechanical systems (MEMS). Etching processes play a critical role in the fabrication schemes of silicon based structures and devices and contribute towards the topography and roughness of the resulting surfaces. Several anisotropic etchants have been used for etching Si surfaces such as potassium hydroxide (KOH), sodium hydroxide (NaOH), lithium hydroxide (LiOH), cesium hydroxide (CsOH) and Tetra methyl ammonium hydroxide (TMAH) [7]. Among these KOH and TMAH are the most popular inorganic and organic etchants as they produce a uniform, bright surface and have high etch selectivity with SiO_2 which is usually used as a mask during the etching process. Several studies have shown that the choice of etchant, etchant concentration, temperature and silicon crystallographic direction affects the roughness of the resulting surfaces [5,8-11]. The degree of anisotropy of the etchants can be changed by the addition of various additives to the anisotropic etching solution [12,13]. The addition of isopropyl alcohol (IPA) to KOH and TMAH solutions was found to result in a visually smooth surface compared to those from pure etchants [14]. The etching characteristics of dry etching methods such as reactive ion etching (RIE) and deep reactive ion etching (DRIE) have also been studied [15,16]. Most of these studies have used optical microscopy or scanning electron microscopy to qualitatively evaluate the roughness of the etched surfaces. However a complete descriptive evaluation of surface roughness parameters was not sought. Some studies employed a profilometer to obtain an average roughness (Ra). A profilometer may not capture the entire frequency spectrum of the roughness due to large probe radius and may also cause localized damage due to high stresses [17]. Atomic force microscopy can

provide high resolution topography image owing to very sharp probe radii, low contact stresses and sub-nanometer displacement detection systems. To the authors' knowledge, very few studies have been focused on the roughness analysis of the etched silicon surfaces using AFM [11,16].

In this paper, we present our investigations on the effect of selected etchants and additives on the surface roughness parameters of the resulting etched silicon surfaces using atomic force microscopy (AFM) and profilometry. Using an AFM provides surface roughness information on length scales pertinent to contact regions in MEMS. Surface roughness evolution spectroscopy (SRES) analysis was carried out to determine the prominent frequencies that arise due to the etching processes. Single asperity and multiple asperity friction experiments of the surfaces were also carried out to evaluate differences in tribological behavior due to difference in roughness. A dry contact model incorporating surface roughness parameters was used to predict real contact area of these surfaces. Correlations between observed tribological behavior and predicted real area of contact are discussed.

3.3 Experimental details:

In all the experiments, n-type silicon (100) wafers were used. The wafers were cut into 1 cm × 1 cm samples and cleaned using the RCA standard clean process [18] before etching to remove the surface contaminants. Hydrogen fluoride (HF) solution was not used during this cleaning process as the removal of the oxide film exposed the Si surface to metallic impurities [19]. The etchants studied were TMAH and KOH. A 25% aqueous solution of TMAH was used at 90 °C. A KOH solution with 8M concentration was used at a temperature

of 80 °C. The effect of adding isopropyl alcohol (IPA) to the etchants on the resulting surface roughness was also studied. The solubility of IPA in KOH solution depends on KOH concentration but in TMAH solution the solubility is unrestricted [14]. For our study, IPA was added to the KOH solution until saturation whereas 20% IPA by volume was added to 25% aqueous TMAH solution. A SiO_2 layer was used as a mask to determine the etch rates of the various etchants. Wafers were thermally oxidized to an oxide thickness of 300 nm and patterns were developed using photolithography to expose a 0.5 cm × 0.5 cm square region of Si. After the etching process the SiO_2 mask was removed by dipping the samples in HF solution. Etch depth analysis was then measured using a profilometer (DEKTAK 11A) with a probe radius of 12.5 μm. All the samples were etched to a depth of about 10 μm. After etching with the anisotropic etchants the quality of the surface was generally poor due to the deposition of the reaction products on the wafer surface [8]. The reaction products were removed using an SPM clean (H_2SO_4:H_2O_2 = 4:1, 90°C) followed by dipping the samples in 37% HCl. The surfaces obtained after the cleaning process were of excellent quality with no contamination. Surface roughness of the etched Si (100) samples was determined using an atomic force microscope (AFM, Dimension™ 3100, Nanoscope IV, Digital Instruments/Veeco Metrology). Surface imaging was carried out in tapping mode under ambient conditions (25 °C, 40% RH) using a silicon tip (tip radius of about 10 nm) at scan sizes of 1 μm × 1 μm, 5 μm × 5 μm and 20 μm × 20 μm with a resolution of 256 × 256 data points per scan. These scan sizes correspond to typical contact and structure sizes in MEMS and the sharp AFM tip can provide information on high frequency roughness. In order to evaluate long range roughness (waviness), 500 μm profiles were also obtained using the profilometer at a lateral resolution of 1 μm.

Single asperity friction measurements were carried out using the AFM with a Si_3N_4 probe (tip radius of 50 nm) in contact mode. The friction response of the tip on a sample was taken to be the difference between the lateral deflection values of forward and reverse scans of a given scan line (i.e. from the friction loop of a scan line). This method is commonly used to eliminate contributions from non-friction sources [20]. The friction value thus noted is a measure of the friction force. The adhesive force between the Si_3N_4 tip and the samples were measured from the force displacement curves. All single asperity friction and adhesive force measurements were conducted at a humidity of 30% RH.

Multiple asperity friction measurements were taken with a ball-on-flat tribometer under linear motion of the sample. A silicon nitride ball with a 1.2 mm radius and surface roughness (RMS) of about 2 nm was rigidly attached to the end of a crossed I-beam structure. This was lowered using a linear stage to apply a normal load to the sample. The normal and frictional lateral forces were measured using semiconductor strain gages and were monitored simultaneously using an ADC card and a personal computer. The samples were affixed to another stage set perpendicular to the beam, providing the linear motion. Each trial was started with the sample stationary, and an initial load of approximately 0.2 mN. The sample was then moved through a distance of 10 mm at 0.6 mm/s as the load was increased to 200 mN.

3.4 Results and discussion:

Figure 1 shows the experimental etch rates of the silicon (100) plane for the etchants used [14]. The etch rates are comparable to results obtained by other groups [7,14,21,22]. The etch

rate of solutions with IPA are slightly lower than the etch rates of the pure solutions. This reduction in the etch rate due to IPA has been attributed to adsorption of IPA at sites on the crystal surface which inhibits the etching reaction [14]. Figure 2 shows typical AFM topography maps obtained on unetched Si (100) and surfaces etched using various etchants at scan sizes of 1 μm × 1 μm, 5 μm × 5 μm and 20 μm × 20 μm. The polished Si wafer has very low roughness and exhibits no discernable features on the surface. The etched surfaces are visually rougher than unetched Si and exhibit pit like structures at 5 μm and 20 μm scan sizes. TMAH appears to produce larger pit like structures than KOH. Typical diameters of these pits at the 20 μm scan size are 2 μm and 3 μm for KOH and TMAH respectively whereas typical depths are 4 nm and 10 nm respectively. The addition of IPA results in more high frequency features at 1 μm scale. However at the 20 μm scale the visual difference in the topography caused by the addition of IPA is less obvious.

We utilized surface roughness spectroscopy (SRES) [23] to characterize and understand the evolution of the Fourier components (spatial frequencies) of the surface roughness caused by various etchants at the 20 μm scale. According to Kim et al. [23], the function $\ln[\hat{h}(\omega_1,\omega_2,t)/\hat{h}(\omega_1,\omega_2,0)]$ gives the roughness evolution of an etched surface where, $\hat{h}(\omega_1,\omega_2,t)$ and $\hat{h}(\omega_1,\omega_2,0)$ correspond to the Fast Fourier Transforms (FFT) of the etched surface and original Si surface respectively. As shown in Fig. 3, the functions $\hat{h}(\omega_1,\omega_2,t)$ and $\hat{h}(\omega_1,\omega_2,0)$ were evaluated numerically using a FFT code and the AFM surface height data at 20 μm. The function $\ln[\hat{h}(\omega_1,\omega_2,t)/\hat{h}(\omega_1,\omega_2,0)]$ is obtained by subtracting the natural logarithm of FFT plots as shown in Fig. 3 and numerically smoothing the data. Figure 4 shows the experimentally measured values of the function $\ln[\hat{h}(\omega_1,\omega_2,t)/\hat{h}(\omega_1,\omega_2,0)$ for

the various etched surfaces. Note that the plots show that the addition of IPA results in a slightly larger range of roughness evolution (the vertical scale for the IPA plots are larger) compared to that of the corresponding pure etchant. For each etchant there are peaks at a particular frequency (wave number) that are enhanced compared to other frequencies. This suggests that features with a particular wavelength become prominent due to etching. We attempted to verify whether these peaks were related to the size of the prominent pit like features seen on the etched surfaces (Fig. 2). The distance between the peaks in the frequency domain is in the order of 1.5 to 3 rad/μm. The prominent wavelength in the frequency domain is calculated using the relation $x = \frac{2\pi}{\lambda}$ where, x is the distance between the peaks and λ is the prominent wavelength. The average pit diameter also was evaluated from 2D analysis of AFM topography maps. Table 2 shows the pit size comparison between the AFM and FFT data. The numbers obtained by the two methods are quite comparable. Moreover both methods indicate similar trends; a) TMAH produces slightly larger pits as compared to KOH and b) etching with additive results in an increase in the pit size as well. These results suggest that SRES analysis can be used to predict prominent feature sizes that arise on an etched surface.

Next, we evaluated the surface roughness parameters of the various surfaces. Surfaces with random surface height distribution and exponential autocorrelation function can be characterized using the amplitude parameters center-line average (R_a), root mean square (RMS), maximum peak to valley distance (PTV), skewness (Sk), kurtosis (K), and the spatial parameter autocorrelation length [24].

For a profile of length L and surface height distribution z(x), the center-line average roughness (R_a) is the arithmetic mean of the absolute values of the vertical deviation from the mean line (m) and is given by

$$R_a = \frac{1}{L}\int_0^L |z - m| dx \qquad (1)$$

The root mean square (RMS or R_q) is the square root of the arithmetic mean of the square of the vertical deviations from the reference line as shown below:

$$RMS^2 = \frac{1}{L}\int_0^L (z - m)^2 dx \qquad (2)$$

Maximum peak to valley distance (PTV) is the distance between the highest asperity and deepest valley of the surface. Skewness (Sk) represents the degree of symmetry of the height distribution about the mean and is equal to the normalized third moment of p(z) about the mean line:

$$Sk = \frac{1}{L\sigma^3}\int_0^L (z - m)^3 dx \qquad (3)$$

where σ is the variance. Note that for a mean line of zero, $\sigma = R_q$. Kurtosis (K) represents the peakedness of the height distribution and is a measure of the number of isolated peaks in the height distribution. Kurtosis is equal to the normalized fourth moment of p(z) about the mean line:

$$K = \frac{1}{L\sigma^4}\int_0^L (z - m)^4 dx \qquad (4)$$

A Gaussian surface distribution has a skewness of zero and a kurtosis of three. Autocorrelation length (ACL) is a measure of randomness of the surface and is the length over which the autocorrelation function [24] drops to 1/e of its original value.

Figure 5 shows the variation of R_a as a function of scan size for the various etched surfaces. All roughness parameter values reported are averages of six measurements at different locations of the sample. Error bars are ± one standard deviation. Note that data at 500 μm was obtained using the profilometer while the other data was obtained using an AFM. For all the samples R_a increases with scan size. This scan size dependence is commonly seen in roughness measurements and is due to large wavelength features (such as waviness) showing up in large scan sizes [25,26]. The data indicated that the etching process results in increases roughness and that TMAH surfaces have higher Ra values than KOH-etched surfaces. Also the addition of IPA results in lower roughness as compared to pure etchants at 500 μm size.

Figure 6 shows the variation of RMS, PTV, skewness and kurtosis as a function of scan size for unetched Si (100) and the various etched surfaces as a function of AFM scan size. RMS and PTV generally increases with scan size which is consistent with previously reported studies [26]. The surfaces etched with the anisotropic etchants have comparable RMS values at scan sizes of 1 μm. At scan sizes of 5 μm and above TMAH exhibits higher roughness than 8 M KOH. Figures 6a-b shows that at 1 μm scan size, surfaces etched with IPA additive results in higher RMS and PTV than surfaces etched with pure etchant. This suggests that IPA acts to enhance high frequency features, which agrees with the observations of topographical features at 1 μm (Fig. 2). However at 5 μm sizes the effect of IPA is less clear. While KOH+IPA continue to result in rougher surfaces than KOH, TMAH+IPA begins to reduce roughness compared to TMAH. The RMS data at 20 μm and R_a data from Fig. 5

suggest that for both KOH and TMAH, IPA helps to reduce long range roughness features resulting in lower average roughness. This is in agreement with the qualitative conclusions reached by others via visual inspection of etched surfaces [14]. The skewness and kurtosis data suggest that the etched surfaces are slightly non-Gaussian. We found no common trend in the variation of skewness and kurtosis with scan size. The etched surfaces generally show more negative skewness at 1 μm and 5 μm scan sizes. At 20 μm scan sizes, surfaces etched with IPA additive show a more positive skewness than surfaces etched with pure etchants. The surfaces show fairly comparable kurtosis values at 1 μm and 5 μm. However at 20 μm, TMAH+IPA etched surfaces results in a significantly lower kurtosis than TMAH-etched surfaces. In the case of KOH, IPA did not have significant effect on the kurtosis even at 20 μm scan size. Figure 7 shows the spatial parameter, autocorrelation length as a function of scan size. The autocorrelation length gives the degree of randomness of the surface [24]. Surfaces with very high degree of randomness have high autocorrelation length. TMAH etched surfaces shows the highest autocorrelation length while KOH etched surfaces show the lowest autocorrelation length. The addition of IPA to TMAH results in a less random surface whereas in the case of KOH, there is no appreciable change.

Next we evaluate the friction characteristics of the various etched surfaces. In the contact of two surfaces contact occurs at numerous contact points. The contact between a sharp AFM tip and the surface simulates single asperity contact. Figure 8(a) shows the single asperity friction behavior of the various surfaces as a function of normal load over a 20 μm scan length. For all samples friction force increases linearly with normal load. Surfaces etched with KOH and TMAH exhibit the highest friction forces. Etching with IPA results in surfaces with lower friction response. Fig. 8b shows the adhesive force of the various

surfaces measured from the force distance curves. The adhesive forces are a combination of the solid-solid adhesion and capillary forces due to surface water layers. From the graphs we note that the adhesive force for surfaces etched using KOH and TMAH are comparable and that they are slightly higher than the unetched Si surface. The trend of the adhesive forces for various surfaces explains their single asperity friction behavior. Etching with IPA acts to reduce the adhesive forces compared to those obtained using pure etchant, thus resulting in reduced friction behavior.

We also measured the friction response of the surfaces using a microtribometer with a Si_3N_4 ball. We verified an elastic contact condition by calculating the plasticity index for the contact between the ball and the various surfaces. The plasticity index (ψ) for an interface predicts the degree of plasticity [24] and is given by

$$\psi = \left(\frac{E^*}{H}\right)\left(\sigma_p \rho_p^*\right)^{1/2} \qquad (5)$$

where E^* is the reduced young's modulus, σ_p is the equivalent asperity standard deviation and ρ_p^* is the equivalent asperity curvature of the two surfaces in contact, and H is the hardness of the softer material (Si). For $\psi < 0.6$, the deformations are largely elastic. For all our surfaces, we obtained an index of 0.14 - 0.18 indicating that our microtribometer data are for elastic contacts. Figure 9a shows the coefficient of friction obtained for the various surfaces. Surfaces etched with IPA show a slightly higher friction response compared to surfaces etched with the pure etchant. This is contrary to the friction behavior observed at the single asperity contact.

For an elastic contact, friction at the micro/nanoscale can be expressed as

$$F_f = \tau A_{re} \qquad (6)$$

where τ is the interfacial shear strength and A_{re} is the real area of contact. In the single asperity friction experiments, A_{re} can be considered constant for all the surfaces. Hence variations in friction force indicate variation in interfacial shear strengths of the interfaces. The data in Fig. 8a would suggest that for a given real area of contact, the surfaces etched with IPA additive should give lower friction force than the surfaces etched with pure etchants. For the loads used in the microtribometer, the contact area was estimated using Hertzian theory to be on the order of hundreds of square microns. At this scale, contact will occur at multiple asperities on the surface and hence real area of contact will depend on the surface roughness parameters [27-30].

We utilized a contact model developed by Kotwal and Bushan [28] to estimate the real area of contact for our samples. This model uses the Pearson system of frequency curves based on the method of moments which provides a family of curves that can be used to generate an equation for a surface height distribution for which the first four moments are known. Pearson defined a criterion *k* given by

$$k = \frac{\mathrm{Sk}^2\,(\mathrm{K}+3)^2}{4(2\mathrm{K} - 3\mathrm{Sk}^2 - 6)\,(4\mathrm{K} - 3\mathrm{Sk}^2)} \qquad (7)$$

where *Sk* and *K* are the skewness and kurtosis of the surface as measured from topography scans. Based on the Hertzian contact size, we used roughness parameters from 20 μm × 20 μm scans of the surface. Depending on the value of *k,* different equations can be obtained for the probability density function [28]. The probability density function is then used in the classical Greenwood and Williamson's model [30] to obtain expressions for the real area of contact, number of contact spots and normal load in terms of the statistical parameters of the

distribution. The normal load (W), real area of contact (A_r) and the number of contacts (n) is given by [28]

$$W = \frac{4}{3}\eta A_a E' R_p \sigma_p^{1.5} F_{1.5}(h) \qquad (8)$$

$$A_r = \pi\eta A_a R_p \sigma_p F_1(h) \qquad (9)$$

$$n = \eta A_a F_0(h) \qquad (10)$$

The standardized separation h, is given by d/σ where d is the separation between the mean planes of the surfaces. E' is the equivalent young's modulus of elasticity and R_p is the equivalent radius of curvature. η, A_a and σ_p are the surface density of asperities, nominal contact area and the equivalent standard deviation of the peak asperities respectively and

$$F_n(h) = \int_h^\infty (s-h)p^*(s)ds \qquad (11)$$

where p* (s) is the height distribution scaled to make its standard deviation unity.

Figure 9b shows the variation of normalized real area of contact as a function of normalized load for the different surfaces at 20 μm scan size. The normalized load is the term $\left[\frac{W}{\eta A_a E` R_p^{0.5} \sigma_p^{1.5}}\right]$; the normalized real area of contact is the term $\left[\frac{A_r}{\pi\eta A_a R_p \sigma_p}\right]$ and the normalized number of contacts is the term $\left[\frac{n}{\eta A_a}\right]$ which is obtained from equations (8), (9) and (10). It can be seen that the normalized real area of contact increases with the normalized loads. Since the real area of contact is normalized with local surface parameters, the slight difference between the various surfaces obtained from the model would be magnified in reality. The results of the model show that for a given load, surfaces etched with

IPA exhibit a higher real area of contact than the surfaces etched with pure etchant. This helps to explain why the surfaces etched with IPA additive exhibit slightly higher friction compared to surfaces with pure etchant. These results indicate that the real area of contact effect dominates friction behavior of the various etched surface at the microscale.

3.5 Conclusions:

This study quantifies and compares surface roughness parameters of silicon surfaces etched with 8M KOH, TMAH with and without IPA additives and evaluates their micro/nanoscale friction behavior. Results showed that although TMAH and KOH produced comparable roughness up to 5 μm scan size, at larger scan sizes TMAH produced rougher surfaces than KOH. The use of IPA additive resulted in enhancement of sub-micron roughness features but a reduction in the long-range roughness of the surfaces to yield smoother surfaces than the pure etchants at scan sizes above 20 μm. All the etched surfaces exhibit pit like features at 20 μm scan sizes. Surface roughness evolution spectroscopy (SRES) showed that TMAH produces slightly larger pits than KOH and using IPA resulted in an increase in the maximum pit size. The single asperity friction behavior correlated well with the adhesive forces for the various surfaces. KOH and TMAH showed comparable behavior and the use of IPA resulted in lower friction forces. However the use of IPA resulted in surfaces with higher real area of contact, which was responsible for higher friction forces in multiple asperity elastic contacts on the microscale. This study demonstrates that the choice of etchants and additives affect the surface roughness and microscale friction behavior of the resulting surfaces.

3.6 Acknowledgments:

The authors would like to thank Prof. Gary Tuttle at the Microelectronics Research Center at Iowa State University for his assistance in etching the samples and for engaging in several constructive discussions during the course of the work. Financial support for the study was provided by a University Research Grant from the Office of the Provost and a grant from the Center for Industrial Research and Service at Iowa State University.

3.7 References:

1. F. Ericson and J. A. Schweitz, "Micromechanical fracture strength of silicon", J. Appl. Phys., 68 (1990) 5840.

2. C. J. Wilson, A. Ormeggi and M. Narbutovskih, "Fracture testing of silicon microcantilever beams", J. Appl. Phys., 79 (1996) 2386.

3. T. Yi, L. Li and C. J. Kim, "Microscale material testing of single crystalline silicon: process effects on surface morphology and tensile strength", Sensors and Actuators, A: Physical, A83 (2000) 172.

4. S. Sundararajan, B. Bhushan, T. Namazu and Y. Isono, "Mechanical property measurements of nanoscale structures using an atomic force microscope", Ultramicroscopy, 91 (2002) 111.

5. R. Maboudian and R. T. Howe, "Critical review: adhesion in surface micromechanical structures", J. Vac. Sci. Technol., B: Microelectronics and Nanometer Structures, 15 (1997) 1.

6. S. Sundararajan and B. Bhushan, "Static friction and surface roughness studies of surface micromachined electrostatic micromotors using an atomic force/friction force microscope", J. Vac. Sci. Technol., A: Vacuum, Surfaces, and Films, 19 (2001) 1777.

7. M. J. Madou, Fundamentals of Microfabrication, CRC Press, New York, 2nd edn. 2002, p.212.

8. I. Zubel, "Silicon anisotropic etching in alkaline solutions II. On the influence of anisotropy on the smoothness of etched surfaces", Sensors and Actuators, A: Physical, A70 (1998) 260.

9. K. Sato, M. Shikida, T. Yamashiro, K. Asaumi, Y. Iriye and M. Yamamoto, "Anisotropic etching rates of single-crystal silicon for TMAH water solution as a function of crystallographic orientation", Sensors and Actuators, A: Physical, A73 (1999) 131.

10. M. Shikida, K. Sato, K. Tokoro and D. Uchikawa, "Differences in anisotropic etching properties of KOH and TMAH solutions", Sensors and Actuators, A: Physical, A80 (2000) 179.

11. N. Miki and S. M. Spearing, "Effect of nanoscale surface roughness on bonding energy of direct-bonded silicon wafers", J. Appl. Phys., 94 (2003) 6800.

12. H. G. Linde and L. W. Austin, "Catalytic control of anisotropic silicon etching", Sensors and Actuators, A: Physical, A49 (1995) 181.

13. C. Moldovan, R. Iosub, D. Dascalu and G. Nechifor, "Anisotropic etching of silicon in a complexant redox alkaline system", Sensors and Actuators, B: Chemical, B58 (1999) 438.

14. I. Zubel and M. Kramkowska, "The effect of isopropyl alcohol on etching rate and roughness of (100) Si surface etched in KOH and TMAH solutions", Sensors and Actuators, A: Physical, A93 (2001) 138.

15. C.-C. Lee and W. Hsu, "Method on surface roughness modification to alleviate striction of microstructures", Journal of Vacuum Science & Technology, B: Microelectronics and Nanometer Structures--Processing, Measurement, and Phenomena, 21 (2003) 1505.

16. S. Chandrasekaran and S. Sundararajan, "Effect of microfabrication processes on surface roughness parameters of silicon surfaces", To appear in Surface Coating and Technology (2004).

17. C. Y. Poon and B. Bhushan, "Comparison of surface roughness measurements by stylus profiler, AFM and non-contact optical profiler", Wear, 190 (1995) 76.

18. G. K. Celler, D. L. Barr and J. M. Rosamilia, "Etching of silicon by the RCA Standard Clean 1", Electrochemical and Solid-State Letters, 3 (2000) 47.

19. R. Divan, N. Moldovan and H. Camon, "Roughening and smoothing dynamics during KOH silicon etching", Sensors and Actuators, A: Physical, A74 (1999) 18.

20. B. Bhushan, Handbook of Micro/Nano Tribology, CRC Press, 2nd edn 1999, 859 pp.

21. I. Zubel and I. Barycka, "Silicon anisotropic etching in alkaline solutions. I. The geometric description of figures developed under etching Si(100) in various solutions", Sensors and Actuators, A: Physical, A70 (1998) 250.

22. K. Sato, M. Shikida, T. Yamashiro, M. Tsunekawa and S. Ito, "Characterization of anisotropic etching properties of single-crystal silicon: Surface roughening as a function of crystallographic orientation", Proceedings - IEEE Annual International Workshop on Micro Electro Mechanical Systems: An Investigation of Micro Structures, Sensors, Actuators, Machines and Systems, 11th, Heidelberg, Jan. 25-29, 1998 (1998) 201.

23. K. S. Kim, J. A. Hurtado and H. Tan, "Evolution of a Surface-Roughness Spectrum Caused by Stress in Nanometer-Scale Chemical Etching", Phys. Rev. Lett., 83 (1999) 3872.

24. B. Bhushan, Principles and Applications of Tribology, John Wiley & Sons, Inc., NY, 1999, p. 99.

25. R. Sayles and T. R. Thomas, "Surface topography as a non-stationary random process", Nature, 271 (1978) 431.

26. V. N. Koinkar and B. Bhushan, "Effect of scan size and surface roughness on microscale friction measurements", J. Appl. Phys., 81 (1997) 2472.

27. F. P. Bowden and D. Tabor, "The friction and lubrication of solids, part I", Clarendon press, Oxford (1950).

28. F. P. Bowden and D. Tabor, "The friction and lubrication of solids,part II", Clarendon press, Oxford (1964).

29. C. A. Kotwal and B. Bhushan, "Contact analysis of non-Gaussian surfaces for minimum static and kinetic friction and wear", Tribol. Trans., 39 (1996) 890.

30. R. Buzio, C. Boragno and U. Valbusa, "Contact mechanics and friction of fractal surfaces probed by atomic force microscopy", Wear, 254 (2003) 917.

31. J. A. Greenwood and J. B. P. Williamson, "Contact of nominally flat surfcaes", Proc. R. Soc., A 295 (1966) 300.

Table 1: Comparison of prominent feature size generated by various etchants at 20 μm scan size between AFM topography and SRES analysis. SRES estimates are comparable to the average pit sizes measured from AFM topography. The estimates also show that pit size increases due to addition of IPA.

SAMPLE	PROMINENT FEATURE SIZE	
	AFM	SRES
8 M KOH	2.4 μm	2.3 μm
8 M KOH+IPA	2.6 μm	2.5 μm
TMAH	3.10 μm	2.5 μm
TMAH+IPA	3.7 μm	4.1 μm

3.8 Figure captions:

Fig 1 Measured etch rates of KOH and TMAH etchants with isopropyl alcohol (IPA) additive and without (pure) in Si (100). The addition of IPA results in a slightly lower etch rate.

Fig 2 AFM topography images of unetched Si (100) and surfaces etched using 8M KOH, 8M KOH+IPA, TMAH and TMAH+IPA at various scan sizes. The etched surface shows pit like features at higher scan sizes. The addition of IPA appears to increase high frequency roughness at the sub-micron scale.

Fig 3 The sequence of steps employed to obtain the surface roughness evolution spectroscopy (SRES) map of an etched surface using AFM topography data (20 μm scan size).

Fig 4 SRES maps of surfaces etched using the various etchants. The lighter regions represent relatively higher magnitude of increase in the roughness. All etchants appear to enhance roughness of a characteristic wavenumber (frequency).

Fig 5 Variation of center line average roughness (R_a) as a function of scan size for various etched surfaces and unetched Si (100). Values were obtained from AFM topography data (1 μm and 20 μm) and from profilometer data (500 μm).

Fig 6 Variation of surface roughness amplitude parameters as a function of scan size for unetched Si and surfaces etched using various etchants obtained from AFM topography data. (a) RMS, (b) peak to valley distance, (c) skewness and (c) kurtosis.

Fig 7 Autocorrelation length as a function of scan size for various etched surfaces obtained from AFM topography data.

Fig 8 (a) Friction force (arbitrary units) as a function of normal load between a Si_3N_4 tip and various etched surfaces, measured using an AFM. (b) Adhesive force data of various surfaces obtained from force distance curves in an AFM. Note that the difference in friction behavior of the various surfaces correlate fairly well with the variation of adhesive forces.

Fig 9 (a) Coefficient of microscale friction between a Si_3N_4 ball and various etched surfaces obtained using a microtribometer. The apparent contact area is on the order of one hundred microns. (b) Normalized real of contact as a function of normalized load for various etched surfaces obtained using a contact model incorporating roughness parameters from 20 μm AFM topography data. Note that for a given load, surfaces etched with IPA result in a higher real area of contact than those obtained with pure etchants.

.

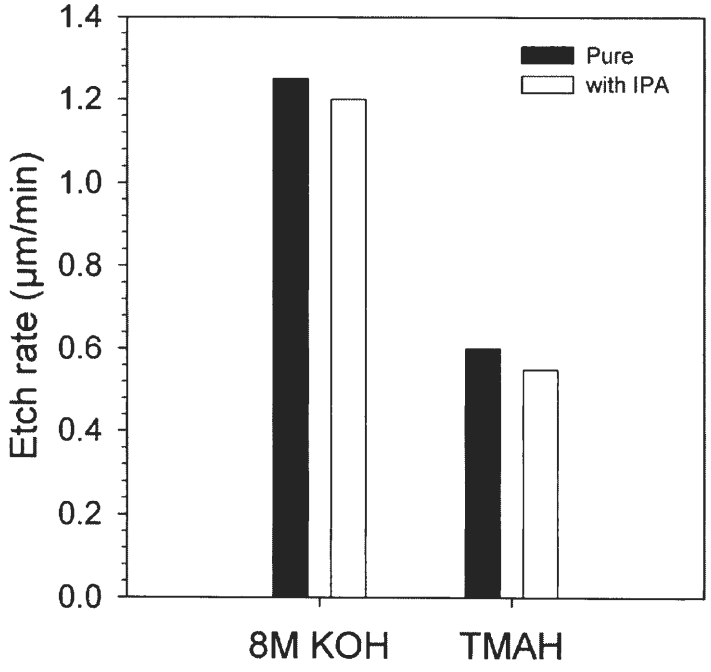

Fig 1

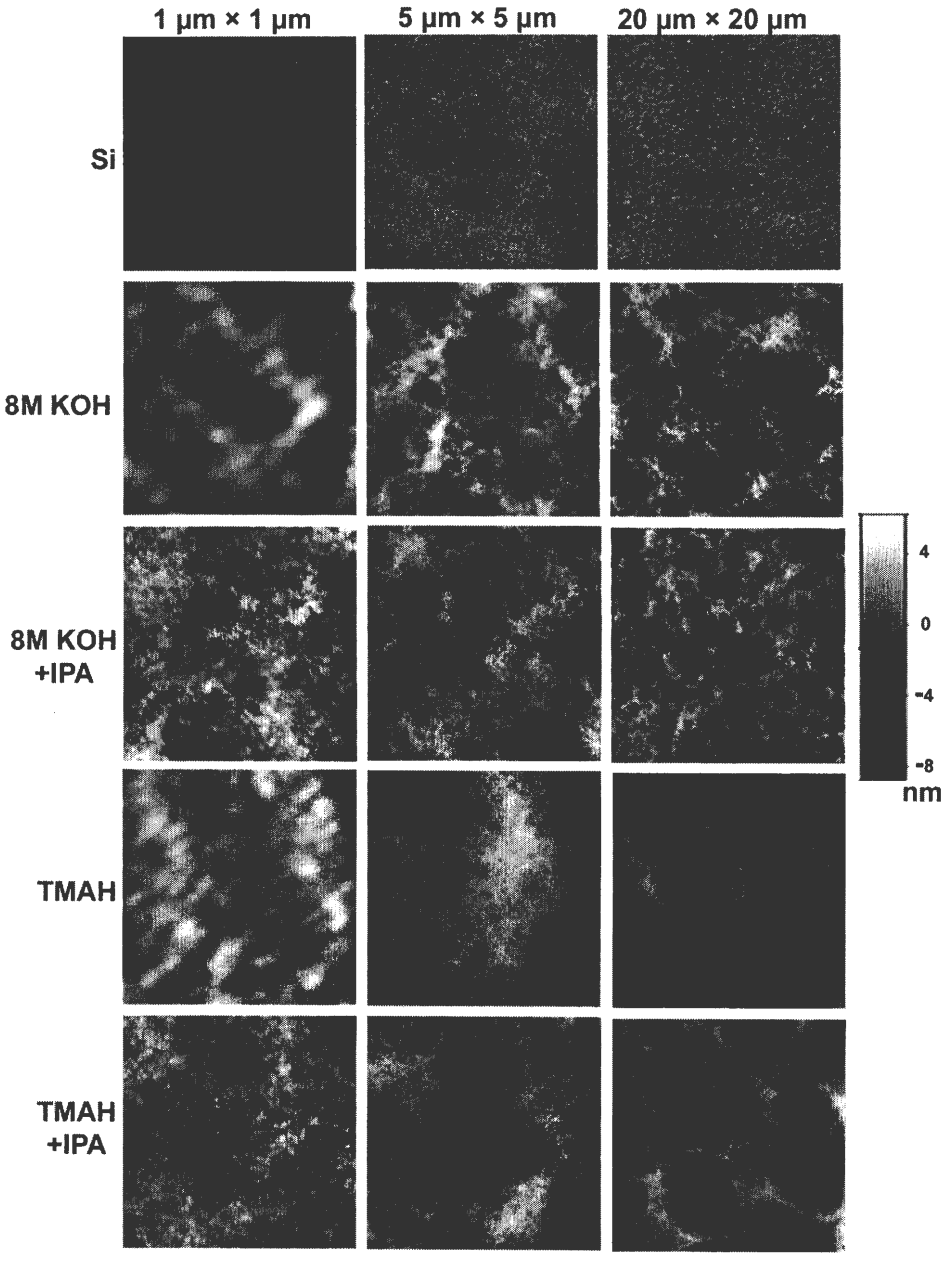
1 μm × 1 μm
5 μm × 5 μm
20 μm × 20 μm
Si
8M KOH
8M KOH +IPA
TMAH
TMAH +IPA
4
0
-4
-8
nm

Fig 2

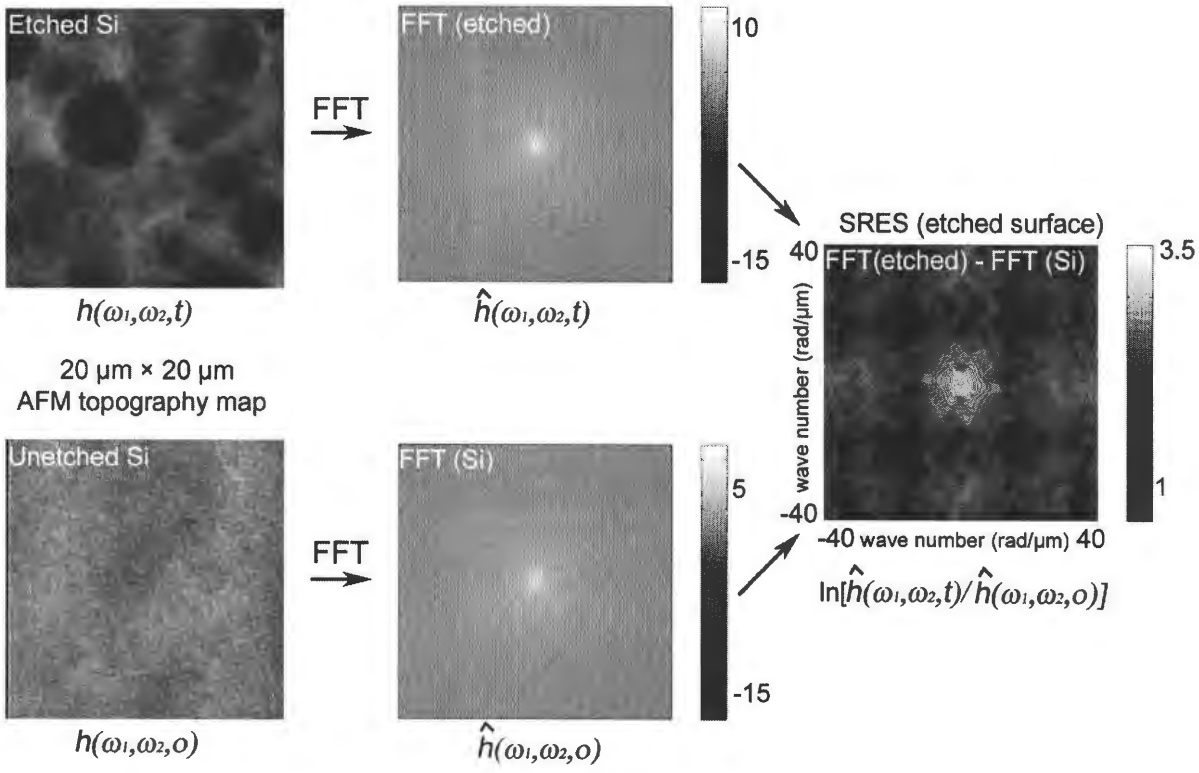
Etched Si
FFT
FFT (etched)
10
-15
SRES (etched surface)
40
FFT(etched) - FFT (Si)
3.5
1
-40
wave number (rad/μm)
-40 wave number (rad/μm) 40
$h(\omega_1,\omega_2,t)$
$\hat{h}(\omega_1,\omega_2,t)$
20 μm × 20 μm
AFM topography map
Unetched Si
FFT
FFT (Si)
5
-15
$\ln[\hat{h}(\omega_1,\omega_2,t)/\hat{h}(\omega_1,\omega_2,o)]$
$h(\omega_1,\omega_2,o)$
$\hat{h}(\omega_1,\omega_2,o)$

Fig 3

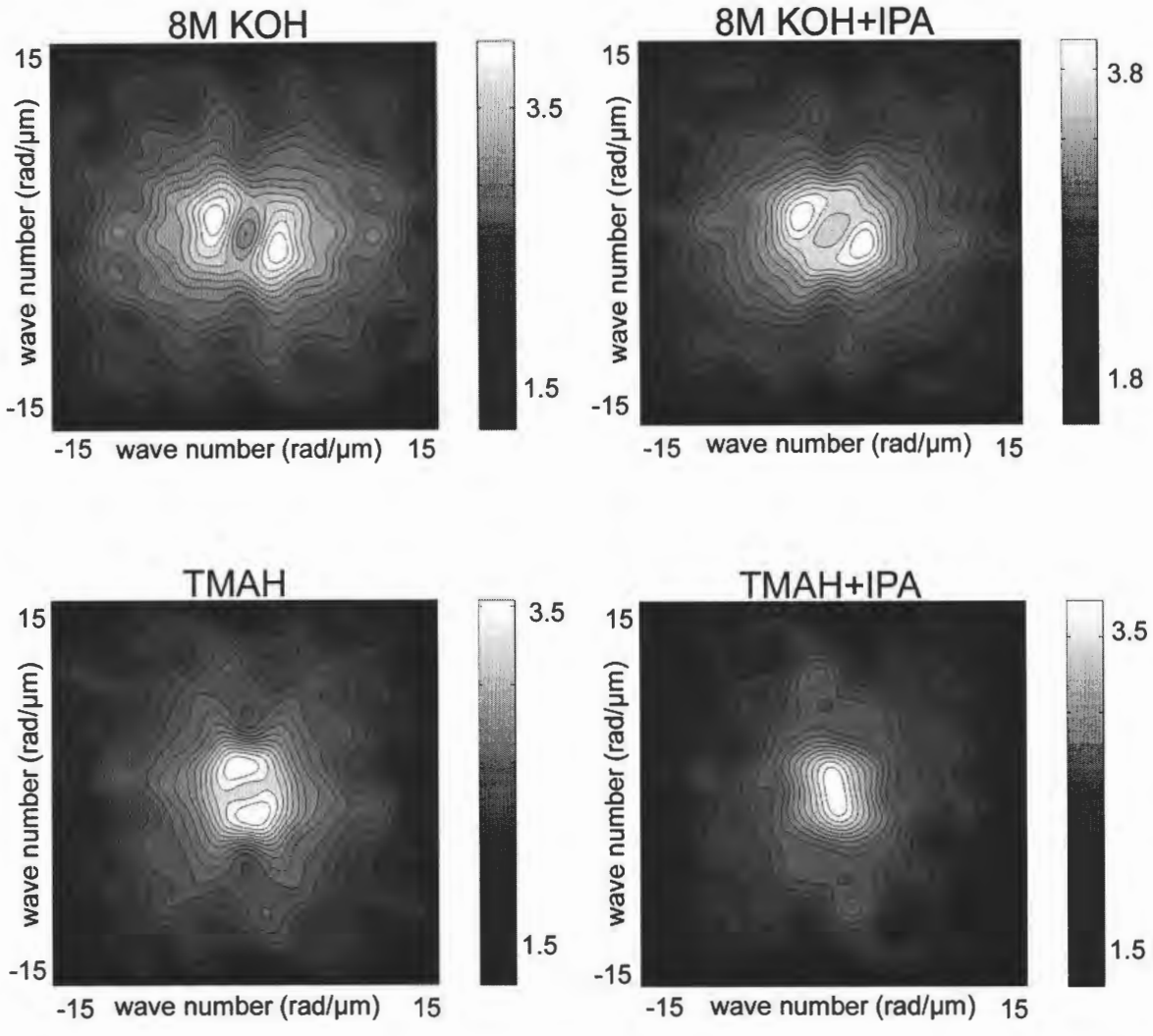
8M KOH
15
wave number (rad/μm)
-15
-15
wave number (rad/μm)
15
3.5
1.5
8M KOH+IPA
15
wave number (rad/μm)
-15
-15
wave number (rad/μm)
15
3.8
1.8
TMAH
15
wave number (rad/μm)
-15
-15
wave number (rad/μm)
15
3.5
1.5
TMAH+IPA
15
wave number (rad/μm)
-15
-15
wave number (rad/μm)
15
3.5
1.5

Fig 4

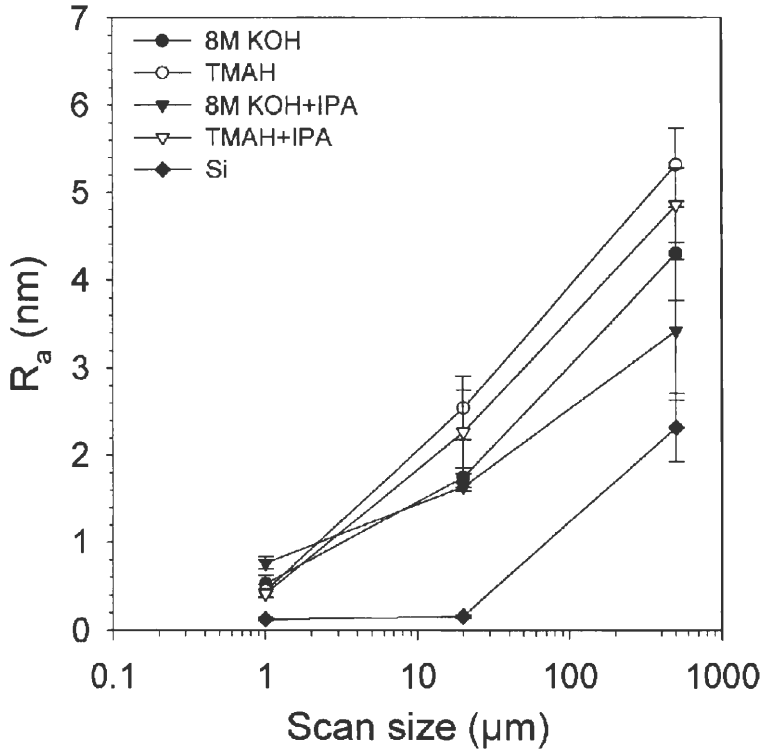
8M KOH
TMAH
8M KOH+IPA
TMAH+IPA
Si
R_a (nm)
0
1
2
3
4
5
6
7
0.1
1
10
100
1000
Scan size (μm)

Fig 5

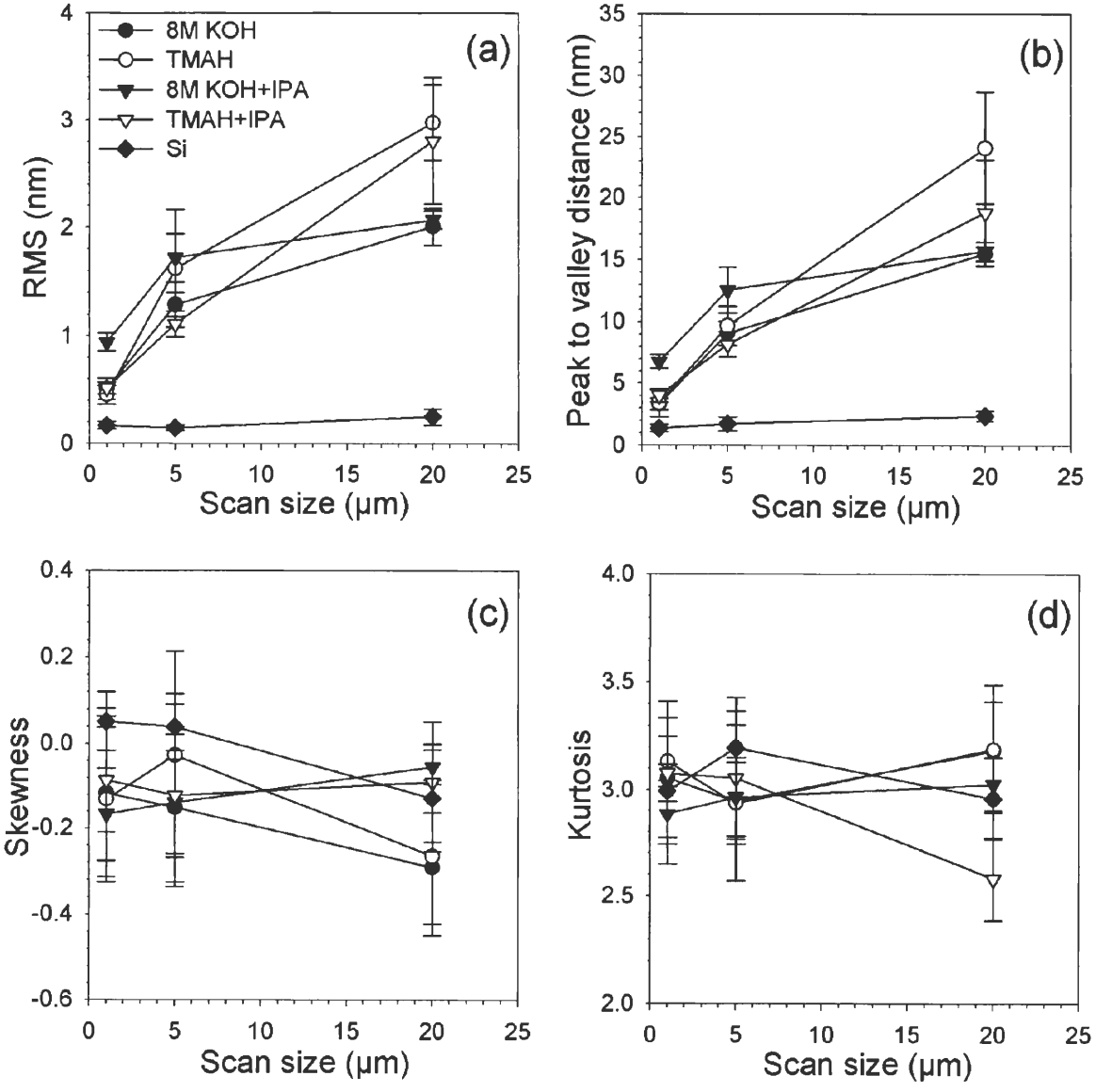
8M KOH
TMAH
8M KOH+IPA
TMAH+IPA
Si
(a)
RMS (nm)
Scan size (μm)
(b)
Peak to valley distance (nm)
Scan size (μm)
(c)
Skewness
Scan size (μm)
(d)
Kurtosis
Scan size (μm)

Fig 6

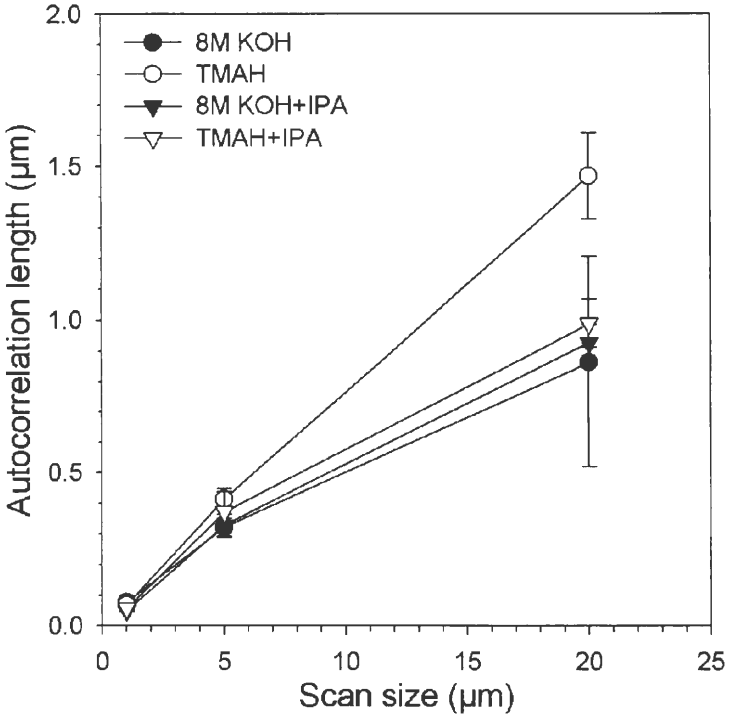
8M KOH
TMAH
8M KOH+IPA
TMAH+IPA
Autocorrelation length (μm)
Scan size (μm)
0.0
0.5
1.0
1.5
2.0
0
5
10
15
20
25

Fig 7

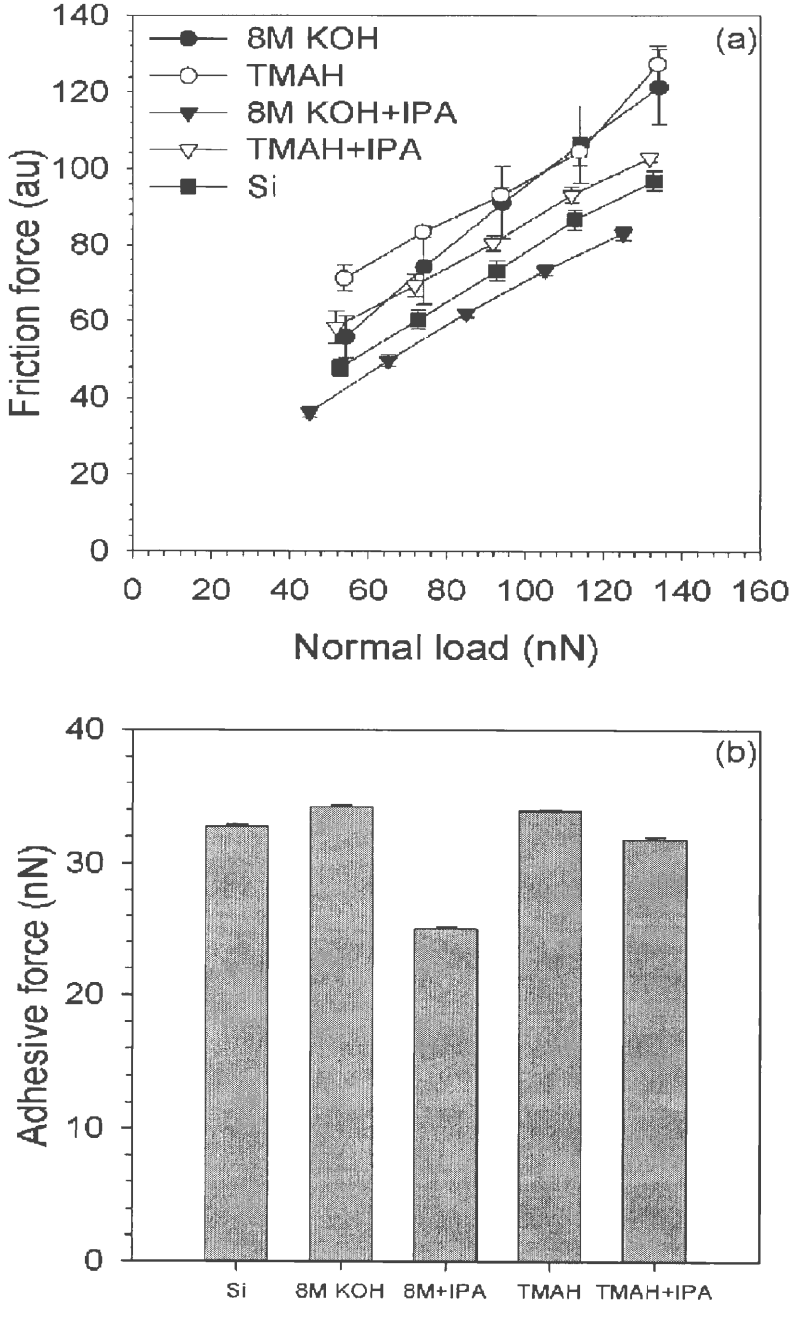
8M KOH
TMAH
8M KOH+IPA
TMAH+IPA
Si
(a)
Friction force (au)
Normal load (nN)
0
20
40
60
80
100
120
140
160
(b)
Adhesive force (nN)
0
10
20
30
40
Si
8M KOH
8M+IPA
TMAH
TMAH+IPA

Fig 8

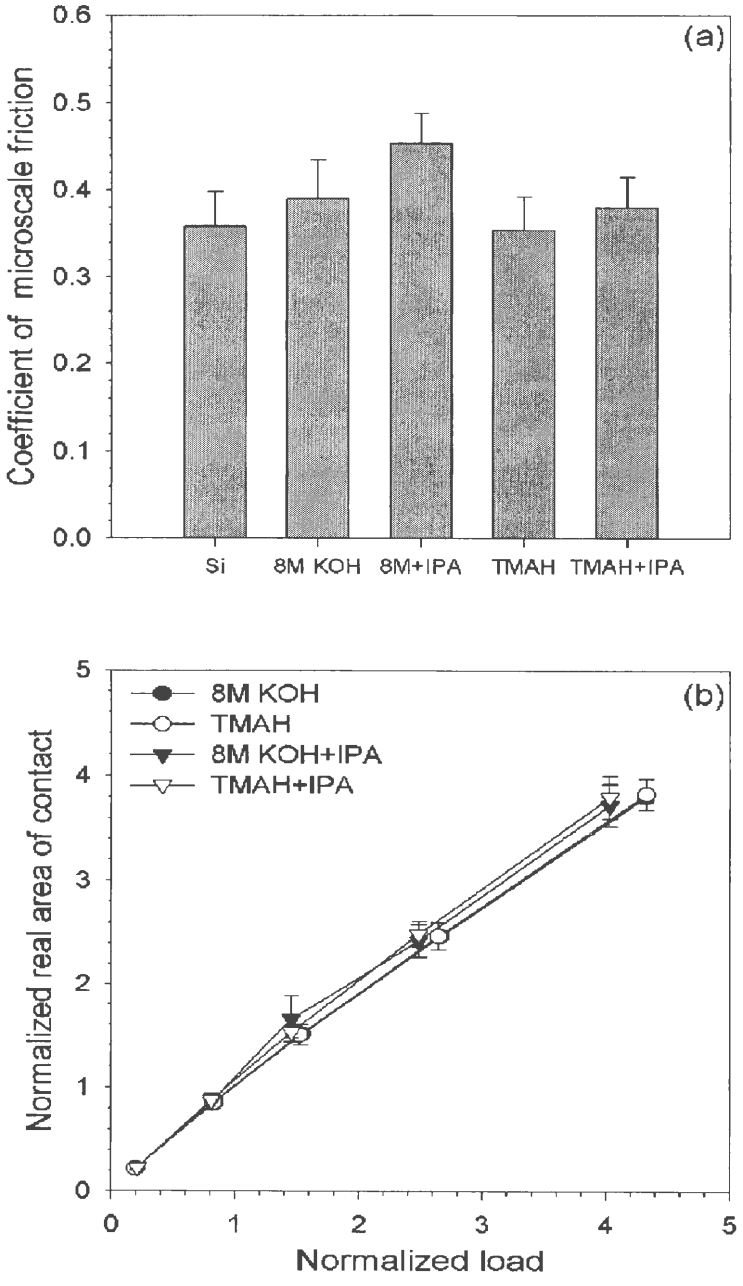
(a)
Coefficient of microscale friction
0.0
0.1
0.2
0.3
0.4
0.5
0.6
Si
8M KOH
8M+IPA
TMAH
TMAH+IPA
(b)
8M KOH
TMAH
8M KOH+IPA
TMAH+IPA
Normalized real area of contact
Normalized load
0
1
2
3
4
5

Fig 9

CHAPTER 4. General conclusions

This study quantifies and compares surface roughness parameters of silicon surfaces etched with KOH (6M, 8M and 10M), TMAH and DRIE. IPA was added to 8M KOH and TMAH and their micro/nanoscale friction behavior was evaluated. Results showed that DRIE produces the smoothest etched surface compared to the anisotropic etchants and also exhibits slightly lower number of contacts at a given load. Hence DRIE would be the preferred method for producing surfaces where surface roughness effects on mechanical properties need to be minimized (e.g. cantilever beams) as well as for surfaces requiring reduced friction/adhesion (e.g. for micromotors). 6 M KOH has high roughness and also exhibits high kurtosis and positive skewness and appears to be the best anisotropic etchant to produce surfaces with low friction. Although TMAH and KOH produced comparable roughness up to 5 μm scan size, at larger scan sizes TMAH produced rougher surfaces than KOH. The use of IPA additive resulted in enhancement of sub-micron roughness features but a reduction in the long-range roughness of the surfaces to yield smoother surfaces than the pure etchants at scan sizes above 20 μm. All the etched surfaces exhibit pit like features at 20 μm scan sizes. Surface roughness evolution spectroscopy (SRES) showed that TMAH produces slightly larger pits than KOH and using IPA resulted in an increase in the maximum pit size. The single asperity friction behavior correlated well with the adhesive forces for the various surfaces. KOH and TMAH showed comparable behavior and the use of IPA resulted in lower friction forces. However the use of IPA resulted in surfaces with higher real area of contact, which was responsible for higher friction forces in multiple asperity elastic contact on the microscale. This study demonstrates that the choice of etchants and additives affect the surface roughness and microscale friction behavior of the resulting surfaces.

APPENDIX

Program to find the autocorrelation distance

```
#include <stdio.h>
#include <stdlib.h>
#include <stdarg.h>

#define ERR_MSG printf
#define DBG_MSG printf


#define MULT_FACTOR (double)1.0e-3

// Input the AFM data file in ASCI format. Remove all the header information and in the first
row of the file input number of rows, number of columns, scan length (μm) and RMS value
(nm) in a single line separated by a space between values

void usage(void)
{
 ERR_MSG("<program> fileName \n file containing 2D matrix in text format should be
given as input \n");
 exit(1);
}

// roftau is the autocorrelation length and tau is the shift distance. Finally roftau is normalized
over sigma
// validate roftau

void validate(double r, int t, double * avg, int *avgCnt)
{

  *avg += r; (*avgCnt)++; //DBG_MSG(" \n Tau: %d  R(tau): %.2f ",t,r);


}


int main(int argc, char* argv[])
{
 FILE *   fpIn = NULL;
 int      nuRows = 0;                    //number of rows
 int      nuCols = 0;                    //number of columns
 double   sampleLength = 0;              //Scan length
```

```
double * matrix = NULL, * temp = NULL;
double   sigma = 0;                          //Measured RMS value
double   mean = 0;
int    row = 0;
int    col = 0;

// We mandatorily need 1 argument
if(argc < 2)
{
 usage();
}

fpIn = fopen(argv[1],"r");

if(NULL == fpIn)
{
 ERR_MSG("\n Unable to Open the input file %s\n",argv[1]);
       exit(1);
}

// First read in the number of rows
if(EOF == fscanf(fpIn,"%d",  &nuRows)) { ERR_MSG("\n File doesnt contain Number of
Rows\n"); exit(1); }
// Read in the number of cols
if(EOF == fscanf(fpIn, "%d", &nuCols)) { ERR_MSG("\n File doesnt contain Number of
Cols\n"); exit(1); }
// Read in scan length
if(EOF == fscanf(fpIn, "%lf", &sampleLength)) { ERR_MSG("\n Length field is
Mandatory\n"); exit(1); }
// Read in Sigma
if(EOF == fscanf(fpIn, "%lf", &sigma)) { ERR_MSG("\n Sigma Field is mandatory\n");
exit(1); }

sigma *= sigma * nuCols;

//write values to output file
DBG_MSG(" \n number of row: %d ",nuRows);
DBG_MSG(" \n number of col: %d ",nuCols);
DBG_MSG(" \n lenght: %.2f ",sampleLength);
DBG_MSG(" \n sigma: %.2f \n",sigma);

// convert the units
//sampleLength *= 1.0e-6; // micro meters
//sigma       *= 1.0e-9; // nano meters
```

```
 // This section reads in the matrix and checks if the number of rows and columns are equal
to the number in the input file

 temp = matrix = (double*)malloc(sizeof(double)*nuRows*nuCols);

 for(row=0;row<nuRows;row++)
 {
  for(col=0;col<nuCols;col++)
  {
   // Read in the element
   //DBG_MSG(" (%d,%d) ",row,col);

if(EOF == fscanf(fpIn,"%lf",temp)) { ERR_MSG("\n Not enuf matrix elements !!\n");
exit(1); }

    // This sections is used to find the mean

    mean += *temp;

    //*temp *= 1.0e-9; // nano meters

    // goto the next element

    temp++;
  }
 }

 mean /= (nuRows*nuCols);

 DBG_MSG(" \n mean: %.2f \n",mean);

//In this section we find ACF for the rows by incrementing the value of tau from 1 to 128 (i.e
half the number of columns)

 {
  int    tau = 0;
  double  roftau = 0;
  double  rowAvg = 0;
  double  colAvg = 0;
  int    rowAvgCnt = 0;
  int    colAvgCnt = 0;

#define ELEMENT(row,col) *(matrix + ((row)*nuCols) + (col))
```

```
for(tau=1;tau<=nuCols/2;tau++)
{
 rowAvg    = (double)0;
 rowAvgCnt = 0;

 for(row=0;row<nuRows;row++)
 {
  roftau = 0;

  for(col=0;col<nuCols-tau;col++)
  {
   roftau += ((ELEMENT(row,col))-mean) * ((ELEMENT(row,col+tau))-mean);
  }

  roftau = (roftau)/sigma;

  validate(roftau,tau, &rowAvg,&rowAvgCnt);
 }

 if(rowAvgCnt)  DBG_MSG("\n %.2f",(double)rowAvg/rowAvgCnt);
}
```

//In this section we find ACF for the columns by incrementing the value of tau from 1 to 128 (i.e half the number of rows)

```
for(tau=1;tau<=nuRows/2;tau++)
{
 colAvg    = (double)0;
 colAvgCnt = 0;

 for(col=0;col<nuCols;col++)
 {
  roftau = 0;

  for(row=0;row<nuRows-tau;row++)
  {
   roftau += ((ELEMENT(row,col))-mean) *  ((ELEMENT(row+tau,col))-mean);
  }

  roftau = roftau/sigma;              //normalize roftau over sigma

  validate(roftau,tau, &colAvg,&colAvgCnt);
 }
```

```
    if(colAvgCnt)  DBG_MSG("\n  %.2f",(double)colAvg/colAvgCnt);
   }

#undef ELEMENT
  }

  fclose(fpIn);

  return(1);

}
```

Program for the contact model

```
#include <iostream.h>
#include <math.h>
#include <stdio.h>
#include <stdlib.h>

void main(){
        int i=0;
```

//Input the AFM data file in ASCI format. Remove all the header information and in the first row of the file input RMS value (nm), skewness, kurtosis and the distance between the mean lines of the surfaces. All the values should be in 1 line separated by spaces.

//Ar is the real area of contact, Sk is the skewness, K is the kurtosis, d is the distance between the two surfaces, A is the apparent area of contact, sigma is the measured RMS value, W is the normal load, C is the number of contacts and pz is the probability density function. smallK, Fo, F1 and F1point5 are parameters defined in the Kotwal and Bhushan's paper (reference number 28 on page 55).

```
        double dummy1=0,dummy2,dummy3;
        double z = 0;
        double Ar = 0;
        double Sk, K, N, d, E, smallK, A, sigmaP;
        double pz, sigma , F1 = 0;
        double F1point5 = 0,Fo = 0, h, W;
        double Rp = 0;
        double C = 0;
        FILE* inputFile;
        const char* filename= "8mipa (2).asc";
```

```
inputFile = fopen(filename, "r");

//read sigma, Sk, K, d

fscanf(inputFile, " %lf %lf %lf %lf " ,&sigma, &Sk, &K, &d);


//calculate smallK

smallK = (Sk*Sk*pow((K+3),2))/(4*(2*K-3*pow(Sk,2)-6)*(4*K-3*pow(Sk,2)));


cout << " d = "<<d<<endl;

while (fscanf(inputFile,"%lf",&z) !=EOF)
{


        //first calculate pz

        pz = 0.3989* exp(-0.5*pow((z/sigma),2));

        //read z and only those z >=d
        //put the values of z in the formulas obtained from kotwal and bhushans paper

        if(z>d){
                F1 = F1 + (((z/sigma)-(d/sigma))*pz);
                F1point5 = F1point5 + ((pow(((z/sigma)-(d/sigma)),1.5))*pz);
                Fo = Fo + ((pow(((z/sigma)-(d/sigma)),0))*pz);

        }

}
```

//substitute the values of F1point5, F1 and Fo in the formulas for W, Ar and C obtained from Kotwal and Bhushans paper//

```
W = (4/3)*N*A*E*pow(Rp,0.5)*pow(sigma,1.5)*F1point5;
Ar = 3.14*N*A*Rp*sigma*F1;
C = N*A*Fo;

cout<<" sigma = "<<sigma<<endl;
cout<<" Fo = "<<Fo<<endl;
cout<<" F1 = "<<F1<<endl;
```

```
        cout<<" F1point5 = "<<F1point5<<endl;
        cout<<" Ar = "<<Ar<<endl;
        cout<<" C = "<<C<<endl;
        cout<<" W = "<<W<<endl;

}
```

ACKNOWLEDGMENTS

I would like to extend my sincere appreciation to my mentor, Dr. Sriram Sundararajan, for his time, patience and guidance in helping me in completing my graduate studies.

I would also like to thank Dr. Pranav Shrotriya and Dr. Gary Tuttle for their help and advice in my academic projects.

A special note of appreciation for my family and friends for their help, love and support.